The Panchromatic Starburst Intensity Limit At Low And High Redshift [1]

Gerhardt R. Meurer, Timothy M. Heckman

The Johns Hopkins University, Department of Physics and Astronomy, Baltimore, MD 21218-2686
Electronic mail: meurer@pha.jhu.edu,heckman@pha.jhu.edu

Matthew D. Lehnert

Sterrewacht Leiden, Postbus 9513, 2300 RA, Leiden, The Netherlands.
Electronic mail: lehnert@strw.LeidenUniv.nl

Claus Leitherer

Space Telescope Science Institute, 3700 San Martin Drive, Baltimore, MD 21218
Electronic mail: leitherer@stsci.edu

James Lowenthal[2]

Lick Observatory, University of California Santa Cruz
Electronic mail: james@lick.ucsc.edu

Accepted for publication in the *Astronomical Journal*.

Received: 10 March, 1997 Accepted: 9 April, 1997

[1]Based on observations with the NASA/ESA *Hubble Space Telescope* obtained at the Space Telescope Science Institute, which is operated by the Association of Universities for Research in Astronomy, Inc., under NASA contract NAS5-26555.

[2]Hubble Fellow.

ABSTRACT

The integrated bolometric effective surface brightness S_e distributions of starbursts are investigated for samples observed in 1. the rest frame ultraviolet (UV), 2. the far-infrared and Hα, and 3. 21cm radio continuum emission. For the UV sample we exploit a tight empirical relationship between UV reddening and extinction to recover the bolometric flux. Parameterizing the S_e upper limit by the 90th percentile of the distribution, we find a mean $S_{e,90} = 2.0 \times 10^{11}\, L_\odot\, \mathrm{kpc}^{-2}$ for the three samples, with a factor of three difference between the samples. This is consistent with what is expected from the calibration uncertainties alone. We find little variation in $S_{e,90}$ with effective radii for $R_e \sim 0.1 - 10$ kpc, and little evolution out to redshifts $z \approx 3$. The lack of a strong dependence of $S_{e,90}$ on wavelength, and its consistency with the pressure measured in strong galactic winds, argue that it corresponds to a *global* star formation intensity limit ($\dot{\Sigma}_{e,90} \sim 45\, \mathcal{M}_\odot\, \mathrm{kpc}^{-2}\, \mathrm{yr}^{-1}$) rather than being an opacity effect. There are several important implications of these results: 1. There is a robust physical mechanism limiting starburst intensity. We note that starbursts have S_e consistent with the expectations of gravitational instability models applied to the solid body rotation portion of galaxies. 2. Elliptical galaxies and spiral bulges can plausibly be built with maximum intensity bursts, while normal spiral disks can not. 3. The UV extinction of high-z galaxies is significant, implying that star formation in the early universe is moderately obscured. After correcting for extinction, the observed metal production rate at $z \sim 3$ agrees well with independent estimates made for the epoch of elliptical galaxy formation.

Subject headings: galaxies: starburst – ultraviolet: galaxies – infrared: galaxies – radio continuum: galaxies – early universe

1. Introduction

Starbursts are regions of intense massive star formation that can totally dominate a galaxy's integrated spectrum. They range in size from giant extragalactic H II regions of scale size ~ 0.1 kpc (e.g. NGC 604 in M 33) to global bursts (often in merging systems) many kpc across that can cover the entire face of the system (e.g. NGC 4038/4039, NGC 4449). There has been much interest in the starburst phenomenon over the past decade or so, yet there is much more to learn. For example we do not know how starbursts are regulated: what turns them on and off, and what keeps them going. Also unknown is how the properties of starbursts vary with size or luminosity. We address some of these issues in this paper.

While starbursts are worthy of investigation in their own right, they are even more important when placed in the broader context of contemporary extragalactic astrophysics. The cosmological relevance of starbursts has been underscored by the recent discovery of: the existence of a population of high-redshift ($z > 2$) UV-bright field galaxies (cf. Steidel *et al.* 1996a,b; Lowenthal *et al.* 1997). The sheer number density of these galaxies implies that they almost certainly represent precursors of typical present-day galaxies in an early actively-star-forming phase. This discovery moves the study of the star-forming history of the universe into the arena of direct observations (cf. Madau *et al.* 1996), and gives added impetus to the quest to understand local starbursts. In particular, a thorough understanding of how to exploit the diagnostic power of the rest-frame ultraviolet (UV) properties of local starbursts will give astronomers powerful tools with which to study star-formation in the early universe.

Accordingly, we have been using the HST to determine the basic UV structure and morphology of starbursts. In our first paper (Meurer *et al.* 1995; hereafter M95) we analyzed in detail UV HST images of nine starburst systems with distances[3] $D < 75$ Mpc. Here, we turn our gaze outward and consider the UV structure of starbursts from $z = 0$ to $z > 3$, in an attempt to document and understand the sytematic properties of starbursts. We also broaden our net by considering the structural properties of infrared-selected "dusty" starbursts.

M95 showed that nearby starbursts are irregular structures consisting of diffusely distributed light interspersed with prominent compact (radii $\leq$ 10 pc) star clusters. Numerous other HST studies have also commented on the presence of luminous young star clusters (including Holtzman *et al.*, 1992; Whitmore *et al.*, 1993; Conti & Vacca, 1994; Hunter *et al.*, 1994; Bower & Wilson, 1995; O'Connell *et al.*, 1995; Whitmore & Schweizer, 1995; Holtzman *et al.*, 1996; Maoz, *et al.* 1996a,b; Schweizer *et al.*, 1996; Watson *et al.*, 1996). While the clusters are certainly the most striking aspect of the images, it is the diffuse light that dominates. M95 find on average 80% of the UV light is diffusely distributed, and 20% comes from clusters. Maoz *et al.* (1996a) find similar fractional UV contributions of clusters in five starburst ring galaxies. M95 argue that there are two modes of star formation in starbursts: prominent cluster formation, and dominant diffusely distributed star formation.

M95 also noted that the effective surface brightnesses of most of the starbursts in their (small) sample span a narrow range of values (dispersion of 0.4 mag arcsec^{-2} for 8/11 starburst regions). Since starbursts produce the most intense UV emission observed in galaxies, this result implies that there is an upper limit to the UV surface brightness of galaxies. Lehnert & Heckman (1996) found a similar limit to the far-infrared surface brightness of far-infrared galaxies (FIRGs). In both samples the illuminating source can be traced to high-mass stars. The

[3]We convert all results to $H_0 = 50\,\mathrm{km\,s^{-1}\,Mpc^{-1}}, q_0 = 0$, except where noted.

UV light studied by M95 is dominated by the light from stars with mass $\sim 20\ \mathcal{M}_\odot$. The far-infrared emission studied by Lehnert & Heckman is thought to result from dust absorbing UV – optical photons (which are predominantly produced by high-mass stars) being heated and reemitting the radiation thermally at infrared wavelengths. Thus FIRGs are thought to be obscured starbursts. These surface brightness limits suggest a limit to the intensity of high-mass star formation, which implies that there is a mechanism that limits the global star formation intensity of galaxies.

Here we reexamine the issue of starburst intensities. Since selection effects are strongest at low surface brightness, we are primarily interested in the intensity maximum. Our aims are to determine what the starburst intensity limit is, investigate whether it varies with certain parameters, and consider what causes the limit. By comparing starbursts selected and observed at different wavelengths we address the issue of opacity and the difference between dusty and relatively dust free starbursts. By comparing starbursts at different redshifts we are able to consider the evolution of starburst intensities, and the resultant cosmological implications. Our method is to compile observations of a diverse set of starburst samples from the literature, combined with (a dash of) new data. After defining some relevant quantities in §2 we compile three samples of starburst data: I. a sample of starbursts observed in the rest-frame vacuum ultraviolet (§3); II. a sample observed in the far-infrared and Hα (§4); and III. a sample observed at radio wavelengths (§5). In §6 we discuss the selection effects and measurement biases, and estimate the level of agreement we expect between intrinsically similar samples. In §7 we discuss the interpretation of the results and their implications, and §8 summarizes the conclusions.

2. Definition of Quantities

To quantify the intensity of high-mass star formation we measure the surface brightness at a wavelength that traces high-mass stars, within an aperture that encompasses half of the *total* emission from the starburst. Thus we employ the effective, or half light, radius R_e, and effective surface brightness S_e enclosed within R_e. These quantities are best measured with a curve of growth extracted from a background-subtracted image of the starburst. Relative to the total luminosity L, the effective surface brightness is given by:

$$S_e = \frac{L}{2\pi R_e^2}. \tag{1}$$

Note that the definition of surface brightness used by Lehnert & Heckman (1996) is a factor of two higher than our definition. Their definition is equivalent to saying that all of the starburst is located within the half light radius of the tracer. Here we assume a one-to-one spatial relationship between the high-mass stars and their trace emission. One complication is that the apertures used to measure R_e are often elliptical, not circular, in shape. Our approach is to take R_e as the geometric equivalent radius of the aperture:

$$R_e = a_e\sqrt{(b/a)_e} \tag{2}$$

where a_e is the semimajor axis length of the elliptical aperture enclosing half the the total flux, and $(b/a)_e$ is the corresponding axial ratio at a_e.

We emphasize that R_e and S_e are global quantities; that is they are associated with the total light of the starburst. This includes both clusters and diffuse light. Furthermore the area over which the S_e is measured scales with the distribution of the light. For moderate to high redshift galaxies full cosmological corrections have been applied to the R_e and L measurements assuming an open universe with $H_0 = 50\,\mathrm{km\,s^{-1}\,Mpc^{-1}}$ and $q_0 = 0$.

The salient properties of starbursts are essentially defined by ionizing stars. These have

masses $\gtrsim 20\ M_\odot$, and hence lifetimes $\lesssim 10$ Myr. Ideally we would like to determine how these stars are distributed. However, the size of the ionizing source distribution is not directly observable since either very little ionizing emission escapes from starbursts, or it is absorbed by the local ISM/IGM before reaching the earth (Leitherer *et al.*, 1996). Therefore R_e of some other tracer of the ionizing population is employed: the vacuum-UV (sample I), Hα (sample II), and 21cm continuum radio emission (sample III). To compare results we convert all flux related measurements to bolometric quantities. The algorithms we use are given below.

To characterize the S_e distribution of a sample we consider the sample median and 90th percentiles, which we denote as $S_{e,50}$ and $S_{e,90}$, respectively. The samples were compiled from a hodge-podge of studies with selection criteria and measurement techniques varying from study to study. In addition, there is a well known bias when observing extended objects to observe those with the highest surface brightness (e.g. Disney 1976; McGaugh *et al.* 1995), so the lower percentiles of the S_e distributions are likely to be rather incomplete. This is especially true for starbursts which are often recognized by their high surface brightness. Therefore, $S_{e,50}$ and $S_{e,90}$ should not be interpreted too literally. They actually represent upper limits to the true median and 90th percentiles of the S_e distributions of star forming galaxies. Here $S_{e,50}$ should be interpreted as the typical surface brightness selected in a sample, and $S_{e,90}$ should be interpreted as close to the highest surface brightness found by a given technique. In §6 we discuss the selection effects and biases of the samples and estimate the level of agreement we expect.

3. Ultraviolet sample

3.1. Ultraviolet extinction

There are many appealing reasons to observe starbursts in the vacuum-UV (see M95). However, there is one serious hindrance to interpreting the results: dust. It efficiently extincts and scatters UV radiation. When dust absorbs UV and optical photons it heats up and reemits the radiation thermally in the far-infrared. The redistribution of radiant energy must be well modeled and corrected for in order to determine the true bolometric luminosity of a starburst.

M95 showed that it is possible to do just that using only the UV properties of starbursts. This is illustrated in Fig. 1 which is adapted from Fig. 6 of M95. It shows the ratio of far-infrared (FIR) flux $F_{\rm FIR}$ to UV flux F_{220} compared to the spectral slope β which is a measure of the ultraviolet color, for a sample of UV-selected starbursts. The definitions of these quantities are given below (§4.1, §3.2) and in M95. In this plot the y axis quantifies the redistribution of spectral energy from the UV to the FIR. A strong relationship is apparent in this diagram - in the sense that, as relatively more light is emitted in the FIR, the starbursts become redder. Note that the hatched region in this plot shows the expected range of colors for naked ionizing populations. All the galaxies in this plot display strong recombination emission spectra, hence their intrinsic colors should be that of an ionizing population. Figure 1 then indicates that reddening is positively correlated with dust extinction. Such a correlation is a major prediction of simple foreground screen models for dust extinction. The dashed line in Fig. 1 shows the expected relationship for a starburst having $\beta = -2.5$ and foreground screen dust having the Calzetti *et al.* (1994; hereafter C94) "extinction law"[4]. Details of the model can be found in M95.

Figure 1 shows that a foreground screen dust geometry models well the redistribution of spec-

[4]We use the term "extinction law" rather loosely. The C94 law is better referred to as an *attenuation law* since it is based on observations which recover most or all of the UV flux, hence extinction is partially compensated for by foreward scattering, thus producing a relatively grey attenuation law.

tral energy from the UV to the FIR. Similar results have been noted by Calzetti *et al.* (1996) and Lehnert & Heckman (1996). However, dust in the vicinity of starbursts does not necessarily have such a simple distribution in all cases. The rms in $F_{\rm FIR}/F_{220}$ about the model line of ~ 0.4 dex is probably larger than the errors, and may be indicative of the non-uniform nature of the dust distribution (e.g. dust lanes). In addition, Fig. 1 plots only UV-selected starbursts, which preferentially will have little extinction.

The point is that the tight empirical relation between UV color and infrared to UV flux ratio shown in Fig. 1 gives us a method to remove the effects of dust extinction for UV-selected starbursts. We adopt the C94 curve in Fig. 1 because it is physically plausible and goes through the data fairly well. Whether or not the details of this model are absolutely correct is irrelevant, as long as this empirical relationship holds for all UV-selected starbursts. Other plausible fits through the data could also be used, and they will yield the same UV correction factor as we derive to within 0.4 dex.

3.2. Calculation of intrinsic quantities

In all cases measurements of L, R_e, and thus S_e have been made from HST images obtained in the rest frame UV. In order to make extinction and k corrections it is crucial to measure the UV color, or equivalently the UV spectral slope, since the observed UV continuum spectra of starbursts are well fit by a power law of index β:

$$f_\lambda \propto \lambda^\beta \tag{3}$$

(C94, M95). Here f_λ is the spectral flux density per wavelength interval. In order to compare the subsamples we reference all observations to the observations of M95. These employed the *Faint Object Camera* with F220W filter, which has central wavelength $\lambda_c = 2320$Å. The total flux is given as $F_{220} = \lambda_c f_{220}$. The methods used to estimate β vary from subsample to subsample, and are described below.

The first step in converting the UV to a bolometric flux is to apply (where appropriate) the k correction:

$$k(220) = \frac{f_{2320}}{f_{\lambda_c/(1+z)}} = \left\{ \frac{(1+z)2320\text{Å}}{\lambda_c} \right\}^\beta . \tag{4}$$

Here λ_c corresponds to the central wavelength of the filters used below. After correcting for Galactic foreground extinction, the UV fluxes were then corrected for intrinsic extinction using the C94 model line in Fig. 1 as discussed above. This model yields the intrinsic extinction $A_{\rm int}$ following the algorithm in M95. For this model a change in spectral slope $\Delta\beta = 0.1$ corresponds to $\Delta A_{\rm int} \approx 0.2$ mag for small $\beta - \beta_0$.

We use the population models of Leitherer & Heckman (1995; hereafter LH95) to convert from intrinsic F220W flux/luminosity to bolometric flux. We assume that starbursts are well represented by a solar metallicity 10 Myr duration constant star formation rate population having a Salpeter (1955) initial mass function (IMF) spanning the mass range of 0.1 to 100 $\mathcal{M}_\odot$. The 10 Myr duration is meant to represent the typical crossing time of a starburst as estimated by M95. Although longer durations are likely in the largest starbursts, the UV properties will be dominated by the stars less than 10 Myr old. In any case the choice of a particular age has only a minor effect on the determination of bolometric quantities. This is demonstrated in Fig. 2 which shows the evolution of $L_{220}/L_{\rm bol}$ at solar metallicity for both instantaneous burst and constant star formation rate populations for this IMF slope (see M95 and LH95 to see the evolution of the numerator and denominator separately). For our adopted population model,

$$\frac{L_{220}}{L_{\rm bol}} = 0.33. \tag{5}$$

Figure 2 shows that for this IMF slope the adopted bolometric correction is accurate to about 20% or better for instantaneous burst populations less

than 10 Myr old (i.e., ionizing bursts) and constant star formation rate populations over the full age range shown. For our adopted starburst population parameters the mass to light ratio is

$$\frac{\mathcal{M}}{L_{\rm bol}} = 2.2 \times 10^{-3} \ \frac{\mathcal{M}_\odot}{L_\odot}, \qquad (6)$$

and the relationship between star formation rate $\dot{\mathcal{M}}$ and $L_{\rm bol}$ is

$$\frac{L_{\rm bol}}{4.5 \times 10^9 L_\odot} = \frac{\dot{\mathcal{M}}}{1 \mathcal{M}_\odot {\rm yr}^{-1}}, \qquad (7)$$

where the luminosity is referenced to $L_\odot = 3.83 \times 10^{33}\,{\rm erg\,s^{-1}}$, the bolometric luminosity of the sun (Allen, 1973). The conversions of light to mass (eq. 6) and star formation rate (eq. 7) are much more dependent on the IMF parameters and adopted star formation history than the bolometric correction (eq. 5), hence our mass and star formation rate estimates should be considered indicative only.

3.3. UV Subsamples

(I.a) Local UV-selected starbursts are represented by the M95 dataset, where the results are derived from HST Faint Object Camera (FOC) images obtained with the F220W filter. Total fluxes and effective radii were determined for the eleven starburst regions observed in nine galaxies (there are three detached regions in their NGC 3690 image). The sample is at sufficiently small redshift that k corrections are unnecessary. The Galactic foreground extinction is taken from Burstein & Heiles (1984), and removed from the UV following the extinction curve of Seaton (1979) using the algorithm given by M95. The β values were measured from *International Ultraviolet Explorer* spectra, and taken directly from M95.

(I.b) We have obtained new data on two starburst galaxies at $z \approx 0.4$, QNY1:32 and SGP1:10, discovered by Boyle *et al.* (1990). The two galaxies were observed with the HST using the FOC and the F342W filter ($\lambda_c = 3403$Å), which has a central wavelength in the rest frame of the galaxies ($\lambda_c/(1+z) \approx 2380$ Å), very similar to that of the F220W filter. The k corrections (eq. 4), although small (< 0.1 mag), were applied. Both galaxies consist of three closely spaced knots aligned nearly linearly. The 512× 512 images were corrected for non-linearity of the FOC and the fluxes and effective radii were obtained from curves of growth using concentric elliptical apertures. The apertures were centered on the central knot and had orientations and axial ratios set to match the outer isophotes of the galaxy. The basic properties of the galaxies are listed in Table 1.

Galactic extinction, listed as $A_{\rm Gal}$ in table 1, was estimated from the foreground H I column density (Stark *et al.* 1992) using the Mathis (1990) extinction curve. These galaxies do not have β or UV color measurements, so we have to estimate $A_{\rm int}$ by some other manner. We have obtained flux calibrated optical spectra for both sources, which confirms that these are indeed starbursts (strong narrow emission lines). The SGP1:10 spectrum was obtained by us with the KPNO 4m telescope. Alexei Filippenko kindly obtained the QNY1:32 spectrum for us using the Lick 3m telescope. The ratio $F_{\rm H\gamma}/F_{\rm H\beta} = 0.46 \pm 0.11$ for SGP1:10, which is consistent with case B recombination and no intrinsic extinction, hence we assume $A_{\rm int} = 0$. Only one Balmer line (Hβ) was well detected in the spectrum of QNY1:32. We assume it has the median reddening $\langle \beta - \beta_0 \rangle = 1.4$ of the rest of the UV sample, hence $A_{\rm int} = 2.2$ mag.

(I.c-e) Very high redshift galaxies are represented by three samples. One was selected from ground based observations, and the other two were from the Hubble Deep Field (HDF) observations (Williams *et al.*, 1996). In all three cases the galaxies were selected as probable Lyman break systems from their broad band colors using the technique pioneered by C. Steidel and collaborators. We consider only the galaxies that have been spectroscopically con-

firmed, which has been done with the Keck telescope in all cases. The confirmation spectra frequently showC IV and Si IV absorption features which are commonly observed in starburst galaxies. These arise in the winds and photospheres of high-mass stars and/or a highly ionized interstellar medium. The crucial size measurements come from HST imagery with WFPC2. The spectral slope β, is measured directly from published broad band colors in the AB system ($m_{\rm AB} = -48.6 - 2.5\log(f_\nu)$, where f_ν is the spectral flux density per frequency interval in units of $\mathrm{erg\,cm^{-2}\,s^{-1}\,Hz^{-1}}$). The redshifts ($z \approx 3$) of the sources put the V to I band observations squarely in the rest frame UV. Details on the individual high-z subsamples are as follows:

(I.c) The original selection for this subsample is from the ground based photometry of Steidel & Hamilton (1992) and Steidel *et al.* (1995). Spectroscopic redshifts are given by Steidel *et al.* (1996a), and HST imagery is reported by Giavalisco *et al.* (1996). There are seven spectroscopically confirmed objects in the sample. Giavalisco *et al.* show that two of the seven galaxies are double. Here we consider the components separately assuming they have a common redshift, so the total size of this subsample is nine. We derive β from the $(\mathcal{G} - \mathcal{R})_{\rm AB}$ colors given by Steidel *et al.* (1996a):

$$\beta = 2.55(\mathcal{G} - \mathcal{R})_{\rm AB} - 2, \qquad (8)$$

We take $R_e = R^T_{1/2}$ from Table 2 of Giavalisco *et al.* (1996).

(I.d) The first HDF sample is that of Steidel *et al.* (1996b). Five confirming redshifts were obtained, one of which corresponds to a double source; thus the total subsample size is six. Effective radii $R_e = R^T_{1/2}$ were taken from their Table 2. Rest-frame UV fluxes were derived from the $\mathcal{R}$ band (combined F606W and F814W light) magnitudes in their Table 1. Finally, β was estimated from the $(m_{\rm F606W} - m_{\rm F814W})_{\rm AB}$ colors given in the HDF version 2 catalog (Williams *et al.*, 1996):

$$\beta = 3.23(m_{\rm F606W} - m_{\rm F814W})_{\rm AB} - 2. \qquad (9)$$

We used $(m_{\rm F606W} - m_{\rm F814W})_{\rm AB}$ in preference to $(m_{\rm F450W} - \mathcal{R})_{\rm AB}$ listed by Steidel *et al.*, because the blue band in the latter may be affected by opacity from the Lyα forest (Madau *et al.*, 1996).

(I.e) The other HDF subsample has confirmation spectra from the DEEP ("Deep Extragalactic Evolutionary Probe") program (Lowenthal *et al.* 1997). A total of 11 high-z detections were made for sources not in sample I.d. Four of these belong to double sources. Hence the total subsample size is 15. Effective radii were taken from their Table 2 (listed as $r_{1/2}$), and β was derived from the $(m_{\rm F606W} - m_{\rm F814W})_{\rm AB}$ colors given in their Table 1 using eq. 9.

3.4. UV results

Figure 3 shows $L_{\rm bol}$ and S_e as a function R_e of the UV-selected samples. The $S_{e,50}$ and $S_{e,90}$ surface brightness levels of the combined sample are plotted as dashed and dotted lines respectively. Figure 4 shows the surface brightness distribution of the combined UV sample in the top panel. The combined sample has $S_{e,90} = 2.0 \times 10^{11}\,L_\odot\,\mathrm{kpc^{-2}}$. Table 1 tabulates $\log(S_{e,50})$ and $\log(S_{e,90})$ levels of the combined UV sample, and its various subsamples.

It is immediately apparent from Fig. 3 that S_e shows little or no dependence on R_e over about two orders of magnitude in size; hence there is no dependence on $L_{\rm bol}$ over about four orders of magnitude in luminosity. Table 1 indicates that $S_{e,90}$ is the same within 0.1 dex for the entire sample and the combined subsamples I.c-e containing just high-z galaxies. This is quite small compared to the cosmological dimming (which has been removed) of $\log(z+1)^4 = 2.4$ dex at $z = 3$.

All of the starbursts in this sample are well resolved; there are no upper limits on size, even though the samples were not biased against point

sources. The range of angular sizes of the galaxies in the samples spans nearly two orders of magnitude similar to the range of absolute sizes. We checked how our results are affected by whether *detached* substructures are counted separately or not by considering the two galaxies in subsample I.b. When their knots are considered separately the brightest in each has S_e about 0.25 dex higher than the galaxy considered as a single unit. However, the average S_e of the individual knots is close to the S_e value of the galaxy as a whole. This indicates that the detached substructures have a high covering factor. We conclude that the S_e measurements are robust to within ~ 0.3 dex with respect to resolution effects.

The same can not be said about the *embedded* structure. In particular the star clusters within starbursts have much higher S_e values than starbursts as a whole. Figure 5 shows $L_{\rm bol}$ and S_e of the star clusters with size estimates from M95 (their table 10). The bolometric corrections were estimated using eq. 5. The $S_{e,50}$ and $S_{e,90}$ lines from Fig. 3 are plotted for comparison. All of these clusters have surface brightnesses above the $S_{e,50}$ and most are above the $S_{e,90}$ level derived from integrated starbursts. This is partially a selection effect since the clusters are all embedded within the dominant diffuse background of a starburst. In this figure there are many upper limits to R_e, and thus lower limits to S_e. In addition the R_e estimates for the clusters in the more distant galaxies are probably inflated (and S_e underestimated) as noted by M95. The most intense emission from a resolved cluster comes from NGC1705-1 with $S_e = 4.7 \times 10^{13}\, L_\odot\, {\rm kpc}^{-2}$. This is over two orders of magnitude more intense than $S_{e,90}$ of the UV sample, yet NGC1705-1 has probably already faded by a factor of ~ 6 from when it was an ionizing cluster (M95, Meurer *et al.*, 1992). Figure 5 demonstrates that high S_e sources can be detected in the UV, they just do not have large scale sizes, nor do they dominate the integrated light of starbursts.

4. Far-infrared - Hα sample

4.1. Subsamples, method

The two subsamples of FIRGs are (II.f) the sample of Armus, Heckman & Miley (1990); and (II.g) the sample of Lehnert & Heckman (1995, 1996). They were drawn from the *IRAS* catalog using the same FIR flux limits used to create the *IRAS* Bright Galaxy Survey (BGS; Soifer *et al.*, 1987, 1989). In addition, these samples have an infrared color selection, $f_{60}/f_{100} \geq 0.77, 0.4$, respectively, where f_{60}, f_{100} are the 60μm and 100μm flux densities from the *IRAS* Point Source Catalog (1988). In order to minimize contamination of the samples by galaxies dominated by active galactic nuclei (AGN) we excluded galaxies with a LINER or Seyfert spectral classification in Veilleux *et al.* (1995).

The FIR luminosity is derived from the far-infrared flux given by

$$F_{\rm FIR} = 1.26 \times 10^{-11} (2.58 f_{60} + f_{100})\, {\rm erg\, cm^{-2}\, s^{-1}}, \quad (10)$$

and the units for f_{60}, f_{100} are Jy (Helou *et al.*, 1985). Almost all of the galaxies in these samples have have $F_{\rm FIR} > F_{\rm optical}$. Hence to a good approximation the bolometric luminosity is equivalent to that produced in the FIR. We take

$$F_{\rm bol} = c(f_{60}/f_{100}) F_{\rm FIR}, \quad (11)$$

where $c(f_{60}/f_{100})$ is the bolometric correction to $F_{\rm FIR}$ to obtain the total FIR luminosity (wavelength range 1-1000 μm). The correction assumes a single dust temperature and emissivity $\propto \nu^{-1}$ and is tabulated by Helou *et al.* (1988). For subsample II.f we assume a single average $c(f_{60}/f_{100}) = 1.5$, on the basis of the f_{60}/f_{100} color range of the sample. For subsample II.g we use the galaxy by galaxy $c(f_{60}/f_{100})$ corrected fluxes given by Lehnert and Heckman (1996). Since the $L_{\rm bol}$ measurements are made in the FIR, no extinction corrections are necessary. For the size of the starburst we take $R_e = R_e({\rm H}\alpha)$, the Hα effective radius.

The Hα images used to estimate R_e were obtained from the ground in FWHM seeing typically 1-2″. Therefore we considered measurements with $R_e < 1.0''$ to be upper limits. There is only one galaxy in the two subsamples with such an upper limit: 01217+0122 with $R_e \leq 0.86''$ from subsample II.f. Its actual S_e value does not significantly affect our results because its limiting $S_e \geq 10^{11}\,\mathrm{L}_\odot\,\mathrm{kpc}^{-2}$ is already greater than $S_{e,90}$ of the combined FIR/Hα sample (see below).

4.2. FIR/Hα results

Figure 6 shows $L_{\rm bol}$ and S_e as a function of R_e for sample II. In comparison to the UV sample, shown in Fig. 3, the FIR/Hα sample looks less like a constant surface brightness correlation. The FIR/Hα sample is richer in low surface brightness galaxies than the UV sample, as can be seen from the surface brightness distribution shown in the second panel of Fig. 4. However, there is little apparent variation in the upper envelope of S_e points in this sample. This illustrates nicely that we are dealing with a surface brightness limit and not a constant surface brightness correlation.

The combined FIR/Hα sample has $S_{e,90} = 0.83 \times 10^{11}\,L_\odot\,\mathrm{kpc}^{-2}$. Table 1 tabulates the $\log(S_{e,50})$ and $\log(S_{e,90})$ values for the two subsamples and the combined FIR/Hα sample. These values for the combined sample are shown as dashed and dotted lines respectively in Fig. 6.

5. Radio sample

5.1. Sample, method

In the radio we use the sample of Condon *et al.* (1990; hereafter C90) which was originally drawn from the *IRAS* BGS. The C90 sample includes over 300 *IRAS* galaxies of all types observed at 21cm with the Very Large Array. The editing steps we apply, which are discussed below, reduce this to a final sample of 38 sources.

To determine the bolometric flux we use the FIR to radio correlation. This well-known correlation (see Helou, 1991, for a review) between fluxes in the two wavelength regimes holds for over four decades in luminosity with an intrinsic scatter of only 0.2 dex making it the tightest correlation in global fluxes of galaxies. Although the physical explanation of the correlation is only now being addressed (e.g. Lisenfeld *et al.*, 1996), it seems to work remarkably well for star formation in all sorts of environments including normal disk galaxies, starburst systems, and even residual star formation in elliptical galaxies. The form of the FIR - radio correlation is:

$$\frac{F_{\rm FIR}}{3.75 \times 10^{12}\,\mathrm{Hz}} = 10^q f_\nu(21\mathrm{cm}) \qquad (12)$$

where $q \approx 2.35$ for starburst and normal galaxies (Sanders & Mirabel, 1996). We adopt this relationship to estimate $F_{\rm FIR}$ and then obtain $F_{\rm bol}$ by bolometric correcting $F_{\rm FIR}$ using eq. 11 and adopting $c(f_{60}/f_{100}) = 1.4$. This is appropriate for the f_{60}/f_{100} ratios of our final radio sample and corresponds to a dust temperature of $T = 45$ K to 70 K, and a ν^{-1} emissivity (Helou *et al.*, 1988).

C90 report 2D-Gaussian fits to the radio images, often for a variety of spatial resolutions and using multiple components. We derive R_e from the angular effective radius taken to be

$$\theta_e = \frac{\sqrt{\theta_M \theta_m}}{2}, \qquad (13)$$

where θ_M and θ_m are the major and minor axis FWHM of the 2D fits. For a true circularly symmetric Gaussian distribution $\theta_e = \theta_M/2 = \theta_m/2$. Condon *et al.* (1991) present higher resolution $\lambda = 3.6$ cm sizes of ultraluminous FIRGs. We chose not to use this study because for most of the galaxies in common to our final sample, the components they resolve only comprise a small fraction of the 3.6 cm flux, or comparisons of the 21 cm and 3.6 cm maps suggest that much diffuse emission is missing from the 3.6 cm maps.

The few remaining galaxies have θ_e that agree to within a factor of ~ 2 at 3.6 and 21 cm.

Four editing passes were done to the sample in order to use well resolved observations and isolate the primary contributor to systems most likely to be starbursts (i.e. not AGN). Firstly, for a given spatial resolution only components with $f_\nu(21\mathrm{cm})/f_\nu(21\mathrm{cm},\mathrm{total}) > 0.5$ were selected so as to reject minor contributors to the total flux. Secondly, for systems observed with with more than one VLA configuration (i.e. at different resolutions) we selected the best resolved observations by taking those with the largest $\theta_M\theta_m/$ [Beam area]. Usually this meant selecting the highest resolution observations. Thirdly, we reject galaxies that do not obey the radio-FIR correlation; from the IRAS and 21 cm fluxes tabulated by C90, we calculate q in eq. 12 and reject sources with $q < 1.9$ as likely radio loud AGN (Sanders & Mirabel, 1996). Finally, in order to exclude other known AGN, we further selected only the systems with H II type spectra in the nuclear regions according to Veilleux *et al.* (1995).

5.2. Radio results

The resulting sample has a relatively narrow 1.5 dex luminosity range centered on $L_{\rm bol} = 2 \times 10^{11}\,L_\odot$. This is primarily due to the final editing step. The BGS subsample used by Veilleux *et al.* (1995) is weighted towards galaxies with $L_{\rm bol} \gtrsim 10^{11}$ (Kim *et al.* 1995), hence low luminosity galaxies were discarded. Rejection of AGN preferentially removes the highest luminosity *IRAS* galaxies (Veilleux *et al.*, 1995; Sanders & Mirabel, 1996). The surface brightness distribution of this sample is shown in the third panel of Fig. 4. The $\log(S_{e,50})$ and $\log(S_{e,90})$ levels are tabulated in Table 1. We find $S_{e,90} = 5.1 \times 10^{11}\,L_\odot\,\mathrm{kpc}^{-2}$ for the radio sample, the highest of the three samples.

In order to determine the effects of the sample editing we calculated $S_{e,50}$ and $S_{e,90}$ at the intermediate editing steps. The most drastic editing step was the final one, paring the sample down from 244 to 38 sources. The sample before this step has $\log(S_{e,90}) = 11.29$, very close to that of the UV sample, but this is due to a large number of sources with $S_e \lesssim 10^9\,\mathrm{L}_\odot\,\mathrm{kpc}^{-2}$. These are largely removed with the H II spectra selection, but also can be removed by applying an infrared color selection as done for sample II; if no H II selection is done, and instead only galaxies with $f_{60}/f_{100} > 0.5$ are selected, the resulting sample is then very similar to our adopted radio sample having $\log(S_{e,50}) = 10.09$ and $\log(S_{e,90}) = 11.64$. The color selection efficiently removes cool low surface brightness emission from the radio sample, but does not discriminate against AGN, which like intense starbursts tend to have high color temperatures. Although we prefer to exclude AGN as best we can, application of the q editing only lowers $S_{e,90}$ by 0.04 dex. This indicates that allowing radio loud AGN to contaminate the sample does not appear to significantly effect the sample $S_{e,50}$ and $S_{e,90}$.

6. Selection effects and biases

All samples are affected by a surface brightness selection. The deepest of the UV subsamples is I.e (Lowenthal *et al.*, 1997). Its limiting magnitude for spectroscopy spread over the typical Keck FWHM $= 0.6''$ seeing disk, corresponds to a limiting $S_e \sim 1.4 \times 10^9\,L_\odot\,\mathrm{kpc}^{-2}$ at $z = 3$, assuming the median value of β. Samples II and III are drawn from the BGS which has a flux limit of $f_{60} = 5.4$ Jy, and is composed primarily of sources unresolved by *IRAS* thus having FWHM $< 2'$. For a typical $f_{60}/f_{100} = 0.55$, this corresponds to $S_e \sim 3 \times 10^7\,L_\odot\,\mathrm{kpc}^{-2}$. The result that none of the galaxies in samples II and III have S_e this low is due to the infrared color selection (sample II) and H II spectrum selection (sample III). The important point is that sample I can not reach the same S_e depth as observed in the other two samples.

The biggest systematic flux uncertainty for the UV sample comes from how we choose to model fig. 1. As noted in §3.1, we expect a ~ 0.4 dex

in $F_{\rm FIR}/F_{220}$ from the scatter in Fig. 1. Indeed if we had used the Kinney *et al.* (1994) extinction curve in our analysis we would have derived $S_{e,50}, S_{e,90}$ to be lower by 0.2 and 0.4 dex respectively for sample I. We have not corrected samples II and III for the fraction of starburst light that escapes dust reprocessing. This should be a small correction since the median $L_{\rm IR}/L_B \approx 5$ for the galaxies in sample II (Lehnert & Heckman 1995; Armus *et al.* 1987). Since much of the B band flux in these galaxies probably arises outside of the starburst we can expect S_e of the starburst to be systematically underestimated by $\lesssim 20\%$.

Quantifying the R_e biases is more difficult, but we can get an idea of the direction they will take. Relative to our stated aim of measuring the R_e of the ionizing population, most of our techniques overestimate R_e due to the effects of the ISM. In principle R_e(UV) provides the most direct estimate of the stellar population size. It may be inflated by extended nebular continuum and scattered light. However M95 show that the former is probably small ($\sim 10\%$ in flux). The resolution of the nearest starbursts into stars argues against scattered light dominating in the UV. Differential extinction (e.g. dust mixed in with the stars) also may inflate R_e(UV) and R_e(Hα). Although in §3.1 we argue that the UV extinction is dominated by a foreground screen (hence extinction will not be differential), M95 note that an idealized uniform screen can not fully describe the dust distribution of most starbursts. R_e(Hα) (sample II) may be more strongly effected by differential extinction than R_e(UV) (sample I), despite the sense of the wavelength difference, because the *IRAS* galaxies are selected to be dusty. In addition, sample II.g is selected by edge-on appearance. Hence, Hα emission may be extincted by cool outer disk dust, far from the starburst, resulting in a large R_e(Hα) bias. We may also expect that R_e(Hα) to be inflated in galaxies displaying galactic winds. However it is not clear that this is a large effect. On the one hand, Marlowe (1997) find that the effect can be a large (factor of five in R_e) in windy blue compact dwarves. On the other hand, using Lehnert's & Heckman's (1995) statistic $\log(\mathrm{R_{H\alpha}}/\mathrm{R}_R)$ we find no noticeable increase of $S_{e,90}$ for subsample II.g when the ten galaxies with the strongest winds are excluded from the subsample. As for sample III, the R_e(21cm) measurements will be least effected by extinction. A bias towards high surface brightness will result from using the Gaussian HWHM to approximate R_e(21cm), instead of doing a full curve of growth analysis, and by using radio interferometric measurements preferentially of high angular resolution. Both procedures discard low surface brightness extended emission. On the other hand, radio emission tends to be more extended than star formation in nearby galaxies (e.g. Marsh & Helou, 1995), probably due to the propagation of cosmic rays in the hosts.

In summary, selection effects and measurement biases may significantly effect the S_e distributions. R_e(UV) and R_e(Hα) are both likely to be inflated with respect to the R_e of the ionizing population; the latter is likely to be more severely affected. Competing physical and measurement biases may cause R_e(21cm) to be either under or overestimated. We expect systematic biases up to a factor of three in UV flux. Agreement of $S_{e,90}$ values to within this factor indicate consistent starburst intensity limits as best we can determine.

7. Discussion

7.1. The Surface Brightness Limit

Table 1 shows that the (full) samples II and III have the largest difference in $S_{e,90}$, 0.8 dex. Since they were originally drawn from the same source, the *IRAS* BGS, the factor of six difference in $S_{e,90}$ is illustrative of the effect that details of final sample selection and measurement bias can have. Since the fluxes used to calculate S_e are essentially the same (tied to $F_{\rm FIR}$), the

differences in $S_{e,90}$ probably arise in the R_e estimates, perhaps for the reasons discussed in §6. The $S_{e,90}$ of sample I splits the difference of the other two samples, agreeing with each to within a factor of three. This is a reasonable level of agreement as discussed above.

We conclude that to better than an order of magnitude, the maximum surface brightness $S_{e,90}$ of starbursts are the same, when deduced from radio, optical and UV observations. We find a mean $S_{e,90} \approx 2.0 \times 10^{11}\, L_\odot\, \mathrm{kpc}^{-2}$ (with a factor of three uncertainty) as the characteristic surface brightness of starbursts, found by averaging in the log the results of the three samples. The lack of a simple wavelength dependence suggests that this is a star formation intensity limit, not an opacity effect. Starbursts orders of magnitude more intense than deduced from UV observations are not common.

Further evidence of the physical significance of $S_{e,90}$ is given by the central pressure P_0 of windy FIRGs. For a sample of 12 galaxies (mostly starbursts) undergoing strong galactic wind Heckman *et al.* (1990) estimate P_0 using the [S II]$\lambda\lambda$6716/6731 Å emission line ratio. They find the mean ($\pm$ dispersion) $P_0 = 2.8 \pm 1.2 \times 10^{-9}\, \mathrm{dy\,cm^{-2}}$. In the starburst models of Chevalier & Clegg (1985), P_0 of a free flowing wind is given by $P_0 = 0.118 \dot{p} R^{-2}$, where $\dot{p}$ is the momentum flux from the starburst, and R is the starburst radius, and the constant is for cgs units. For our standard starburst population model (§3.2) the momentum flux due to supernovae and stellar winds is given by

$$\dot{p} = 2.1 \times 10^{23} \frac{L_{\mathrm{bol}}}{L_\odot}\, [\mathrm{erg\,cm^{-1}}]. \qquad (14)$$

The constant varies by a factor of 1.6 for burst durations in the range of 5 to 100 Myr. The star formation intensity required to produce P_0 is then

$$\frac{S_e}{10^{11}\, L_\odot\, \mathrm{kpc}^{-2}} = \frac{P_0}{1.63 \times 10^{-9}\, \mathrm{dy\,cm^{-2}}}. \qquad (15)$$

Hence the mean value of P_0 measured by Heckman *et al.* (1990) corresponds to $S_e = 1.7 \times 10^{11}\, L_\odot\, \mathrm{kpc}^2$. This is very close to the adopted $S_{e,90}$, but derived using methods completely independent of those in §3 - §5.

Since we are measuring the surface brightness of star formation tracers, we can convert $S_{e,90}$ to an equivalent star formation intensity ($\dot{\mathcal{M}}$ per unit area) of

$$\dot{\Sigma}_{e,90} \sim 45\, \mathcal{M}_\odot\, \mathrm{kpc}^{-2}\, \mathrm{yr}^{-1} \qquad (16)$$

using eq. 7 (and bearing in mind the caveats of Sec. 3.2). Strictly speaking the observed emission is dominated by high-mass star formation. If the lower mass limit of our adopted Salpeter IMF is 5 $\mathcal{M}_\odot$, then $\dot{\Sigma}_{e,90}$ is reduced by a factor of 5.5.

Because selection effects preferentially depopulate low S_e sources, 90% *or more* of starbursts have $S_e \lesssim 2.0 \times 10^{11}\, L_\odot\, \mathrm{kpc}^{-2}$. Thus it is close to an upper limit to the surface brightness of starbursts. This implies that starbursts with $S_e \approx S_{e,90}$ can only be more luminous by being larger. The UV results in particular show that the same limit applies over two orders of magnitude in R_e (four in L) and displays little evolution out to $z \approx 3$.

The star formation intensity is much higher in starbursts relative to that integrated over typical galactic disks. This is illustrated in the bottom panel of Fig. 4 which shows the S_e distribution of normal disk galaxies, derived from the Hα imaging sample of Ryder & Dopita (1993). Here bolometric fluxes due to high-mass star formation were derived from Hα fluxes using the Zanstra method. R_e estimates were kindly provided by S.D. Ryder, and correspond to the effective radius of the elliptical aperture containing half of the total Hα emission. Table 1 lists $S_{e,50}$, and $S_{e,90}$ for this sample. The typical S_e of star formation in normal spiral galaxies is about three orders of magnitudes fainter than that of commonly selected starbursts. Much of the difference can be ascribed to the filling factor of star formation. The Hα morphology of normal spiral

galaxies is characterized by numerous, but widely separated H II regions, whereas starburst galaxies are typically dominated by a single central super-bright star forming complex. Individual giant H II regions in normal galaxies may have S_e approaching that found in starbursts.

7.2. Starburst Regulation

What are the regulating mechanisms that limits the global starburst intensity? The central pressure estimates discussed above suggests that feedback from high-mass star formation may be involved in the regulation (cf. the discussion of M82 by Lehnert & Heckman 1996). However, it is unclear how this would regulate star formation intensity. The near equivalence between $R_e(\mathrm{H}\alpha)$ and the rotation curve turn-over radius $R_{\rm to}$ found by Lehnert & Heckman (1996) suggests that the global dynamics of the host in limiting at least the size of the starburst. Here we consider whether the S_e limit is related to the stability of inner disks of galaxies.

Following on the work of Toomre (1964) and Quirk (1972), Kennicutt (1989) showed that the radial gas surface density profiles $\Sigma_g(R)$ in spiral galaxies closely follows, but is somewhat under, the surface density at which gas disks would be unstable to their own self gravity. Specifically, Kennicutt defines the critical density for star formation as

$$\Sigma_c = \frac{\alpha\kappa\sigma}{3.36G} \tag{17}$$

where σ is the velocity dispersion of the gas, $\alpha = 0.67$ is an empirically determined constant, and

$$\kappa = \left(R\frac{d\Omega^2}{dR} + 4\Omega^2 \right)^{1/2} \tag{18}$$

is the epicyclic frequency for angular frequency $\Omega = V(R)/R$ with $V(R)$ being the rotation curve. He found that massive star formation in H II regions seems to be inhibited except where $\Sigma_g > \Sigma_c$. The so called "Kennicutt law" has proven to be very successful in determining the location of H II regions (or lack of them) in a variety of galaxies including the normal spirals, low surface brightness galaxies (van der Hulst *et al.*, 1993), and H II galaxies (Taylor *et al.*, 1994). The overall success of the Kennicutt law (however cf. Ferguson *et al.*, 1996; Meurer *et al.*, 1996) implicates self gravity in regulating star formation in gaseous disks.

Kennicutt's original calibration of α was done for galaxies with star formation in the flat part of the rotation curve. What happens in the rising portion of the rotation curve where starbursts occur? Assuming a simple linear rise, Ω is constant (solid body rotation), and we have $\Sigma_c = \alpha\sigma\Omega/(1.68G)$. We assume that $\Sigma_g \approx \Sigma_c$, since in the Kennicutt scenario, once Σ_g reaches or surpasses Σ_c, star formation becomes relatively efficient, thus regulating Σ_g. This assumption certainly holds in particular cases, such as NGC 3504, where Σ_g traces Σ_c well into the solid body portion of the rotation curve (Kenney *et al.*, 1993). On causality grounds, the quickest time-scale expected for star formation is the dynamical time-scale given by

$$t_{\rm dyn} = \sqrt{\frac{3\pi}{16G\rho}} \tag{19}$$

(Binney & Tremaine, 1987) where ρ is the mean interior density. Note that, for a cold massless disk in the potential of a dominant spherical mass distribution, the solid body portion of the rotation curve corresponds to a constant density core. In that case $t_{\rm dyn} = \frac{1}{2}\pi\Omega^{-1}$. The maximum star formation intensity expected for gas at Σ_c is then

$$\dot{\Sigma}_c \leq \frac{\Sigma_c}{t_{\rm dyn}} = 9 \times 10^{-5}\, \alpha\sigma\Omega^2\ [\mathcal{M}_\odot\,{\rm yr}^{-1}\,{\rm kpc}^{-2}], \tag{20}$$

where σ is in units of $\mathrm{km\,s^{-1}}$, and Ω is in units of $\mathrm{km\,s^{-1}\,kpc^{-1}}$. This can be expressed in terms of bolometric surface brightness using eq. 7:

$$S_c \approx 4.0 \times 10^5\, \alpha\sigma\Omega^2\ [L_\odot\,{\rm kpc}^{-2}], \tag{21}$$

using the same units as eq. 20. Figure 7 plots S_e versus Ω for the galaxies in Lehnert & Heckman

(1996). There is a weak correlation (correlation coefficient $R = 0.61$) in the sense predicted by eq. 21, which is plotted for $\alpha = 0.67$, $\sigma = 15$ $\mathrm{km\,s^{-1}}$ (the central H I velocity dispersion of a representative normal disk galaxy; Dickey *et al.*, 1990). More importantly, almost all the galaxies in this sample have $S_e < S_c$ as expected. We conclude that our results are consistent with Kennicutt's threshold model of star formation. This implies that starbursts may be regulated by the same gravitational instability mechanism that applies to the outer disks of galaxies. The extraordinary nature of starbursts is not due to extraordinary physics. Rather it is due to the high densities required to reach the instability limit, and the consequent short minimum dynamical time-scales (see also Elmegreen, 1994).

Although application of the Kennicutt law is insightful, it does not explain why the same surface brightness limit appears to hold over two orders of magnitude in size. It suggests that the blame should be shifted to a fundamental limit on the angular frequency Ω, or to the central density since $\rho_0 \propto \Omega^2$. But we have no insight into whether such a limit really exists, or why it should exist. It also does not explain the efficiency of star formation. We conclude that the stability of a gaseous disk against self gravity probably plays an important role in limiting starburst intensity, but in and of itself is not sufficient to explain the S_e limit of starbursts.

7.3. Galaxy formation

How does $S_{e,90}$ relate to the global star formation history of normal galaxies? Can they be made in a high intensity starburst? Normal galaxies also show preferred surface brightnesses. Bright spirals obey the Freeman (1970) law having exponential disks with extrapolated B band central surface brightnesses of $B(0)_c = 21.65$ mag arcsec^{-2}, which translates to an effective surface brightness of $S_e = 5.1 \times 10^7 L_{\mathrm{B},\odot}\,\mathrm{kpc}^{-2}$. McGaugh *et al.* (1995) showed that this is actually an upper limit to the surface brightness distribution of disk galaxies when selection effects are taken into account. Elliptical (E) galaxies fall on the so-called "fundamental plane" in $\log(R_e)$, $\log(S_e)$, and $\log(\sigma)$. Using the fundamental plane projections of Djorgovski & Davis (1987) we estimate the properties of a representative low-luminosity E galaxy to be $R_e = 1.2$ kpc, $\sigma = 180\,\mathrm{km\,s^{-1}}$, and $S_e(r_G) = 9.0 \times 10^8 L_{r_G,\odot}\,\mathrm{kpc}^{-2}$, whereas for a representative high-luminosity E galaxy we adopt $R_e = 12$ kpc, $\sigma = 350\,\mathrm{km\,s^{-1}}$, and $S_e(r_G) = 1.4 \times 10^8 L_{r_G,\odot}\,\mathrm{kpc}^{-2}$. Here the observations are defined in the r_G passband (Djorgovski, 1985).

An estimate of the minimum time needed to build a galaxy (e.g. at the starburst intensity limit) is given by

$$t_{\mathrm{build}} = \frac{(M/L)S_e}{\dot{\Sigma}_{e,90}}\,\mathrm{Myr}, \qquad (22)$$

where $\dot{\Sigma}_{e,90}$ is given in eq. 16. Taking $M/L_B \approx 2.5$ to be appropriate for spirals (Puche & Carignan, 1991) and $M/L_{r_G} \approx 5$ for E galaxies (Djorgovski & Davis, 1987) yields $t_{\mathrm{build}} \approx 3$, 98, and 15 Myr for spirals, low luminosity E and high luminosity E galaxies respectively.

As before, the minimum time-scale for star formation will be on the order of the dynamical time. This is given by

$$t_{\mathrm{dyn}} \approx \frac{2R_e}{\sigma} \approx \frac{2R_e}{V_{\mathrm{circ}}} \qquad (23)$$

(following equation 4-80b in Binney & Tremaine, 1987). Taking $R_e = 1.68\alpha_B^{-1}$ (Freeman, 1970) and using the data of Puche & Carignan (1991) typically $t_{\mathrm{dyn}} \sim 60$ Myr for spiral galaxy disks. Using the representative E galaxy parameters listed above, $t_{\mathrm{dyn}} \approx 13, 67$ Myr for low and high luminosity E galaxies respectively.

We see that t_{build} is on the order of, or larger than, t_{dyn} for E galaxies, and so it is plausible that they were made by a maximum intensity starburst – this scenario would not violate burst duration limits set by causality. It is thought

that the epoch of E galaxy formation is at $z \gtrsim 1$ (e.g. Bender *et al.*, 1996), hence it is plausible that the high-z starbursts are elliptical galaxies forming. This issue is further addressed below.

Spiral disks, on the other hand, have $t_{\rm build} \ll t_{\rm dyn}$, so a maximum intensity burst would produce many more stars in a dynamical time-scale than are observed in spiral disks. These considerations are in accord with observations of present day disk galaxies which indicate that star formation occurs on a few Gyr or longer time-scale (Kennicutt *et al.*, 1994). Although maximum intensity bursts are too strong to build disks, disk galaxies usually have central high surface brightness bulges. Bulges fall on the fundamental plane and thus they can be made by maximum intensity bursts. Indeed, the surface brightness profiles of central starburst galaxies are somewhat akin to those of spiral galaxies, but with the "bulge" being blue and corresponding to the starburst (cf. Schade *et al.* 1996; Lilly *et al.* 1995).

7.4. Extinction in high redshift galaxies

In §3 we showed that there is little apparent z evolution in S_e of the UV-selected sample. One of the most important corrections we make to the UV data is the extinction correction which turns out to be substantial. Here we explore whether these corrections are reasonable, and the implications arising from the extinction correction.

Figure 8 shows the distribution of β values for the low and high redshift galaxies. Here we plot only one point in the cases where a galaxy was separated into multiple starburst components, since the same β estimate was used for all components in these cases. The arrows show the intrinsic $\beta_0 = -2.5$ for an unreddened ionizing population, and the median β of the sample. The median shifts by less than 0.05 in β if the local sample is excluded. Furthermore, the range of observed β is virtually identical at high and low redshifts. The high-z starbursts thus have very similar UV color distributions to the low-z sample.

Figure 8 illustrates that most starbursts, including the high-z ones, are redder than naked ionizing populations. The high-z samples are selected to have the bluest possible rest-frame UV colors. Young unreddened populations will preferentially be selected if they exist. Either there are very few high-z galaxies dominated by ionizing populations, and/or some of the ionizing populations are reddened.

Opacity from the Lyα forest may redden the photometric β values, if the blue filter in the color index samples rest wavelengths bluewards of 1216Å. This is likely to be a problem only for subsample I.c. Excluding this subsample changes the median β by less than 0.05. Hence Lyα forest opacity is not the reddening mechanism.

Our interpretation is that the reddening is due to dust extinction. We know this is valid for the local UV sample (see Fig. 1). Unfortunately the confirmation spectra of the high-z galaxies do not extend to the rest-frame optical where the emission lines should be strong, allowing confirmation of the presence of an ionizing population. The same rest frame UV absorption features are seen in both the low and high-z samples, however they are relatively narrow in the high-z sample (Lowenthal *et al.*, 1997), so it is not clear whether they have a stellar or interstellar origin. Hence, we can not rule out the possibility that the high-z sample is contaminated by older non-ionizing stellar populations. It is unlikely that there is significant contamination by faded starbursts, because aging has a more severe effect on luminosity than our extinction corrections. It will take ~ 400 Myr after a starburst turns off for it to redden to the observed median $\beta = -1.1$, during that time it will have faded by a factor of ~ 500 (assuming the burst duration $\ll 400$ Myr; see Fig. 16 of M95), whereas the extinction correction for this β is a factor of eight in the F220W band. Hence, post-bursts would have been that much brighter when they were ionizing populations, and such ultra-luminous starbursts are not detected at high-z. More worrisome is

contamination by extended duration star forming populations. However, durations longer than 300 Myr are required to reach the median β even if the IMF slope is $\alpha = 3.3$ (LH95). If contamination is severe we would have the curious effect that S_e and β evolution "conspire" to mimic no evolution and a simple extinction correction. We prefer the simpler interpretation that the same physical mechanism, extinction by dust, reddens both the low and high-z starbursts.

The top axis of Fig. 8 translates β to extinction at 1620Å (the approximate rest wavelength of the HDF observations longward of the Lyman Limit) using the C94 extinction law. The median extinction is 2.9 magnitudes at this wavelength (a factor of 15 in flux). For the Kinney *et al.* (1994) extinction law, the median extinction would be 2.0 magnitudes. In either case, the extinction is substantial.

In their pioneering paper, Madau *et al.* (1996) use these high-z galaxies to evaluate the metal enrichment history of the early universe deriving *apparent* metal ejection rates $\dot{\rho}_Z(z) = 3.6,\ 0.62,\ 1.1\ \times 10^{-4}\,\mathrm{M}_\odot\,\mathrm{yr}^{-1}\,\mathrm{Mpc}^{-1}$ at $z = 2.75, 3.25, 4$ (see Madau *et al.* for details). They note that these values are underestimates because (1) they do not sample the full luminosity function, (2) they represent only the least dusty systems, and (3) they assume no dust extinction in their analysis. We can improve on their work by correcting their results for the median $A_{1620} = 2.9$ mag extinction seen in starbursts. This yields $\dot{\rho}_Z(z) = 54, 9.4, 17 \times 10^{-4}\,\mathrm{M}_\odot\,\mathrm{yr}^{-1}\,\mathrm{Mpc}^{-1}$ for the above three redshifts. Strictly speaking these results are still lower limits to the true $\dot{\rho}_Z(z)$ of the universe.

Figure 9 shows our revised version of the $\dot{\rho}_Z(z)$ evolution diagram (cf. Fig. 9 of Madau *et al.*). Here we adopt the flat cosmology used by Madau *et al.* $H_0 = 50\,\mathrm{km\,s}^{-1}\,\mathrm{Mpc}^{-1}$, $q_0 = 0.5$, and assume $\Lambda = 0$. The x axis here is look-back time in linear units, and the y axis is linear in $\dot{\rho}_Z(z)$. All data points are shown as lower limits: the high-z data because completeness corrections still have not been addressed; and the data with $z < 1$ because they have not been corrected for extinction. If the extinction correction to the other points is small, then our new estimates suggest that the epoch of peak galaxy formation may be as early as $z \approx 3$. Clearly much work needs to be done to put all estimates of $\dot{\rho}_Z(z)$ on the same scale.

Our new estimates of $\dot{\rho}_Z(z)$ are well above the mean metal ejection rate of the universe $\langle\dot{\rho}_Z\rangle \approx 4.2 \times 10^{-4}\,\mathrm{M}_\odot\,\mathrm{yr}^{-1}\,\mathrm{Mpc}^{-1}$ (Madau *et al.*, 1996). Strictly speaking it too is a lower limit, since it neglects low surface brightness galaxies and intergalactic and intracluster gas in the estimation. Mushotzky & Loewenstein (1997) provide an estimate of $\langle\dot{\rho}_Z\rangle = 3.4 \times 10^{-3}\,\mathrm{M}_\odot\,\mathrm{yr}^{-1}\,\mathrm{Mpc}^{-1}$ in the redshift interval $z = 1$ to 6 – the epoch of elliptical galaxy formation. This level is plotted as a dashed line in Fig. 9. In Madau *et al.* it seemed possible that the universe was relatively quiescent at high redshifts. It now appears that the universe was forming stars, and producing metals, at a high rate at $z > 2$. Our results imply that rather than a quiescent universe we are observing an active but moderately obscured early universe.

8. Summary

We have examined a diverse set of observations of starburst galaxies, spanning six decades of wavelength, sizes ranging from ∼0.1 to 10 kpc, and redshifts out to $z = 3.5$. The observations were used to estimate effective radii R_e, total luminosities L, and effective surface brightnesses S_e on the bolometric scale. The samples were drawn from observations obtained in 1. the rest frame space ultraviolet (UV), 2. the far-infrared and Hα (FIR/Hα), and 3. 21cm radio emission. The UV data, which spans the largest range in z, were consistently corrected for dust extinction as estimated from the UV reddening of the starbursts. We have demonstrated that this correction adequately models the redistribution of radiation from the UV to the FIR in nearby starbursts.

The extinction in the UV is significant. High-z galaxies observed in the rest frame UV are too red to be naked starbursts. If this reddening is due to dust, the typical implied extinction is $\sim$ 2 to 3 mag at $\lambda = 1620$Å. The corrected metal production rate at $z \gtrsim 3$ is then $\dot{\rho}_Z \gtrsim 2 \times 10^{-3}\,\mathcal{M}_\odot\,\mathrm{Mpc}^{-3}\,\mathrm{yr}^{-1}$, about five times or more higher than Madau *et al.*'s (1996) estimate of the Hubble time averaged $\langle\dot{\rho}_Z\rangle \approx 4.2 \times 10^{-4}\,\mathcal{M}_\odot\,\mathrm{Mpc}^{-3}\,\mathrm{yr}^{-1}$, but in good agreement with Mushotzky & Loewenstein's (1997) estimate of $\langle\dot{\rho}_Z\rangle \approx 3.4 \times 10^{-3}\,\mathcal{M}_\odot\,\mathrm{Mpc}^{-3}\,\mathrm{yr}^{-1}$ during the epoch of elliptical galaxy formation. Depending on the amount of extinction required for the data having $z < 2$, the peak in $\dot{\rho}_Z(z)$ could be pushed back to $z \gtrsim 2$. Applying plausible extinction corrections illustrates that rather than being quiescent, much of the star formation in the early universe may be obscured.

The upper limit to the surface brightness of starbursts is parameterized by $S_{e,90}$ - the 90th percentile surface brightness of the samples. This statistic is susceptible to systematic uncertainties due to measurement biases and the heterogeneous sample selection. We find that the samples have the same $S_{e,90}$ to within a factor of three. This is about the level of agreement we expect for intrinsically similar samples affected by known flux biases. We conclude that to within a factor of a few the same $S_{e,90}$ applies to both dusty and relatively unobscured starbursts, it does not vary with size for $R_e \gtrsim 0.1$ kpc, and shows little evolution out to $z \approx 3.5$.

Our adopted 90th percentile surface brightness limit is the mean value (in the log) $S_{e,90} \approx 2.0 \times 10^{11}\,L_\odot\,\mathrm{kpc}^{-2}$ of the three samples. The absence of a strong wavelength variation of $S_{e,90}$ indicates that it corresponds to a physical limit on star formation intensity, rather than being an opacity effect. Further evidence of the physical significance of $S_{e,90}$ comes from the central ISM pressure $P_0 = 2.8 \pm 1.2 \times 10^{-9}\,\mathrm{dy\,cm}^{-2}$ measured in galaxies (mostly starburst) undergoing a strong galactic wind by Heckman *et al.* (1990). Using the models of Chevalier & Clegg (1985) and Leitherer & Heckman (1995), the corresponding surface brightness of the stellar population pressurizing the ISM is $S_e = 1.7 \times 10^{11}\,L_\odot\,\mathrm{kpc}^2$. This is identical to $S_{e,90}$, but is derived from completely different considerations.

Our adopted $S_{e,90}$ corresponds to a star formation intensity of $\dot{\Sigma}_{e,90} \sim 45\mathcal{M}_\odot\,\mathrm{kpc}^{-2}\,\mathrm{yr}^{-1}$. Since starbursts represent the most intense star formation in the universe, and since selection effects depopulate low S_e sources, these values of $S_{e,90}$ and $\dot{\Sigma}_{e,90}$ parameterize the maximum *global* intensity of star formation observed in the universe. Within starbursts there are localized sources with $S_e \gg 2 \times 10^{11}\,L_\odot\,\mathrm{kpc}^{-2}$. These are star clusters. However, their integrated light does not dominate starburst emission, and their sizes are limited to $R_e \lesssim 10$ pc. The intense cluster forming mode of star formation apparently does not operate for $R_e \gtrsim 0.1$ kpc.

Our results imply that some robust mechanism is limiting the global intensity of starbursts. The P_0 comparison implicates mechanical energy feedback from supernovae and stellar ejecta in regulating starbursts. We also examined the consequences of disk stability models (e.g. Kennicutt, 1989) to the central portions of galaxies where the rotation curve is solid body like and most starbursts are observed to occur. There we expect an upper limit to $S_e \propto \sigma\Omega^2 \propto \sigma\rho$, where σ is the gas velocity dispersion in the disk, Ω is the angular frequency, and ρ is the spherical volume density. We show that most starbursts with rotation curve data obey this limit for an adopted central velocity dispersion $\sigma = 15$ $\mathrm{km\,s}^{-1}$. This model implies that starbursts have higher S_e than normal disk galaxies because the star formation occurs in the center of galaxies where the critical density is high and the star formation time-scale is short. Unfortunately, this model (while illuminating) does not explain the constancy of $S_{e,90}$, it only casts it in terms of a limit on Ω or the central value of ρ.

Normal galactic disks could not have been

made in a maximum intensity burst because it would have been accomplished in much shorter than the dynamical time scale $t_{\rm dyn}$, the minimum time set by causality arguments. However, bulges, which often dominate the center of disk galaxies, can be made in a maximum intensity burst without violating such causality limits. The same goes for elliptical galaxies. Considering the R_e and L of the high-z galaxies, and the agreement of the corrected metal production rate derived from them with that expected at the epoch of E galaxy formation, it is tempting to speculate that at $z \approx 3$ we are witnessing the formation of elliptical galaxies (Giavalisco *et al.* 1995).

Acknowledgements: Numerous astronomers watched this work develop and provided useful hints of samples to include, and other suggestions. In particular we would like to thank Mark Dickinson, Mauro Giavalisco, Jeff Goldader, Piero Madau, Stuart Ryder, Nick Scoville, Min Yun, and Esther Zirbel. Asao Habe, Chris Mihos, Colin Norman, and Rosie Wyse provided useful comments on earlier drafts of this paper. We are grateful to Alexei Filippenko for obtaining the QNY1:32 spectrum for us. Jim Condon saved us a lot of effort by emailing us data from C90. We are grateful for the support we received from NASA through HST grant number GO-05491.01-93A and LTSA grant number NAGW-3138. This paper is in large part based on observations with the NASA/ESA *Hubble Space Telescope* obtained at the Space Telescope Science Institute, which is operated by the Association of Universities for Research in Astronomy, Inc., under NASA contract NAS5-26555. Literature searches were performed using NED, the NASA/IPAC Extragalactic Database, a facility operated by the Jet Propulsion Laboratory, Caltech, under contract with the National Aeronautics and Space Administration.

REFERENCES

Allen, C.W. 1973, *Astrophysical Quantities, Third Edition*, (Athlone, London)

Armus, L., Heckman, T.M., & Miley, G.K. 1987, AJ, 94, 831

Armus, L., Heckman, T.M., & Miley, G.K. 1990, ApJ, 364, 471

Bender, R., Ziegler, B., & Bruzual, G. 1996, ApJ, 463, L51

Binney, J., & Tremaine, S. 1987, *Galactic Dynamics*, (Princeton University Press, Princeton)

Bower, G.A., Wilson, A.S 1995, ApJS, 99, 543

Boyle, B.J., Fong, R., Shanks, T., and Peterson, B.A 1990, MNRAS, 243, 1

Burstein, D., & Heiles, C. 1984, ApJS, **54**, 33

Calzetti, D., Kinney, A.L., & Storchi-Bergmann, T. 1994, ApJ, 429, 582 (C94)

Calzetti, D., Kinney, A.L., & Storchi-Bergmann, T. 1996, ApJ, 458, 132

Carozzi, N. 1977, A&A, 55, 261

Carozzi-Meyssonnier, N. 1978, A&A, 63, 415

Chevalier, R.A., & Clegg, A.W. 1985, Nature, 317, 44

Condon, J.J., Helou, G., Sanders, D.B., & Soifer, B.T. 1990, ApJS, 73, 359 (C90)

Condon, J.J., Huaung, Z.-P. Yin, Q.F., & Thuan, T.X. 1991, ApJ, 378, 65.

Conti, P.S., Vacca, W.D. 1994, ApJ, 423, L97

Dickey, J.M., Hanson, M.M., & Helou, G. 1990, ApJ, 352, 522

Disney, M.J. 1976, Nature, 263, 573

Djorgovski, S. 1985, PASP, 97, 1119

Djorgovski, S., & Davis, M. 1987, ApJ, 313, 59

Durret, F. & Bergeron, J. 1988, A&AS, 75, 273

Elmegreen, B.G. 1994, ApJ, 425, L73

Ferguson, A.M.N., Wyse, R.F.G., Gallagher, J.S. III, Hunter, D.A. 1996, AJ, 111, 2265

Freeman, K.C. 1970, ApJ, 160, 811

Gallego, J., Zamorano, J., Aragón-Salamanca, A., & Rego, M. 1995, ApJ, 455, L1

Giavalisco, M., Maccheto, F.D., Madau, P., & Sparks, W.B. 1995, ApJ, 441, L13

Giavalisco, M., Steidel, C.C., & Macchetto, F.D. 1996, ApJ, 470, 189

Heckman, T.M., Armus, L., & Miley, G.K. 1990, ApJS, 74, 833

Helou, G., Soifer, B.T., & Rowan-Robinson, M. 1985, ApJ, 298, L7

Helou, G., Khan, I.R., Malek, L., & Boehmer, L. 1988, ApJS, 68, 151

Helou, G. 1991, in *The Interpretation Of Modern Synthesis Observations Of Spiral Galaxies*, edited by N.C. Duric, & P. Crane, (Astronomical Society of the Pacific, San Francisco), p. 125

Holtzman, J.A., Faber, S.M., Shaya, E.J., Lauer, T.R., Groth, E.J, Hunter, D.A., Baum, W.A., Ewald, S.P., Hester, J.J., Light, R.M., Lynds, R., O'Neil, E.J. Jr., Westphal, J.A. 1992, AJ, 103, 691

Holtzman, J.A., Watson, A.M., Mould, J.R., Gallagher, J.S. III, Ballester, G.E., Burrows, C.J., Clarke, J.T., Crisp, D., Evans, R.W., Griffiths, R.E., Hester, J.J., Hoessel, J.G., Scowen, P.A., Stapelfeldt, K.R., Trauger, J.T., Westphal, J.A. 1996, AJ, 112, 416

Hunter, D.A., O'Connell, R.W., Gallagher, J.S. 1994, AJ, 108, 84

IRAS Point Source Catalog, ver. 2. 1988. Washington: GPO

Kenney, J.D.P., Carlstrom, J.E., & Young, J.S. 1993, ApJ, 418, 687

Kennicutt, R.C. 1989, ApJ, 344, 685

Kennicutt, R.C., Tamblyn, P., & Congdon, C.E. 1994, ApJ, 435, 22

Kim, D.-C., Sanders, D.B., Veilleux, S., Mazzarella, J.M., & Soifer, B.T. 1995, ApJS, 98, 129

Kinney, A.L., Calzetti, D., Bica, E., & Storchi-Bergmann, T. 1994, ApJ, 429, 172

Lehnert, M., & Heckman, T.M. 1995, ApJS, 97, 89

Lehnert, M., & Heckman, T.M. 1996, ApJ, 472, 546

Leitherer, C., & Heckman, T.M. 1995, ApJS, 96, 9 (LH95)

Leitherer, C., Ferguson, H.C., Heckman, T.M., Lowenthal, J.D. 1996, ApJ, 454, L19

Lilly, S.J., Hammer, F., Le Fèvre, O., & Crampton, D. 1995, ApJ, 455, 75

Lilly, S.J., Le Fèvre, O., Hammer, F., & Crampton, D. 1996, ApJ, 460, L1

Lisenfeld, U., Völk, H.J., & Xu, C. 1996, A&A, 306, 677

Lowenthal, J.D., Koo, D.C., Guzmán, R., Gallego, J., Phillips, A.C., Faber, S.M., Vogt, N.P., Illingworth, G.D., & Gronwall, C. 1997, ApJ, *in press*

Madau, P., Ferguson, H.C., Dickinson, M.E., Giavalisco, M., Steidel, C.C., & Fruchter, A. 1996, MNRAS, 283, 1388

Maoz, D., Barth, A.J., Sternberg, A., Filippenko, A.V., Ho, L.C., Macchetto, F.D., Rix, H.-W., Schneider, D.P. 1996a, AJ, 111, 2248

Maoz, D., Filippenko, A.V., Ho, L.C., Macchetto, F.D., Rix, H.-W., Schneider, D.P. 1996b, ApJS, 107, 215

Marlowe, A.T. 1997, Ph.D. Thesis, The Johns Hopkins University

Marsh, K.A., & Helou, G. 1995, ApJ, 445, 599

Mathis, J.S. 1990, ARA&A, 28, 37

McGaugh, S.S., Bothun, G.D., & Schombert, J.M. 1995, AJ, 110, 573

Meurer, G.R., Freeman, K.C., Dopita, M.A., & Cacciari, C. 1992, AJ, 103, 60

Meurer, G.R., Heckman, T.M., Leitherer, C., Kinney, A., Robert, C., & Garnett D.R. 1995, *Astron. J.*, 110, 2665 (M95)

Meurer, G.R., Carignan, C., Beaulieu, S., & Freeman, K.C. 1996, AJ, 111, 1551

Mushotzky, R.F., & Loewenstein, M. 1997, ApJ, *accepted*

O'Connell, R.W., Gallagher, J.S. III, Hunter, D.A., Colley, W.N. 1995, ApJ, 446, L1

O'Connell, R.W., & Mangano, J.J. 1978, ApJ, 221, 62

Peterson, C.J. 1980, PASP, 92, 397

Puche, D., & Carignan, C. 1991, ApJ, 378, 487

Quirk, W.J. 1972, ApJ, 176, L9

Rubin, V.C., Thonnard, N., Ford, W.K., & Burstein, D. 1982, ApJ, 261, 439

Ryder, S.D., & Dopita, M.A. 1993, ApJS, 88, 415

Salpeter, E.E. 1955, ApJ, 121, 161

Sanders, D.B. & Mirabel, I.F. 1996, ARA&A, 34, 749

Schade, D., Lilly, S.J., Le Fevre, O., Hammer, F., & Crampton, D. 1996, ApJ, 464, 79

Schweizer, F., Miller, B.W., Whitmore, B.C., Fall, S.M. 1996, AJ, 112, 1839

Seaton, M.J. 1979, MNRAS, 187, 73p

Soifer, B.T., Sanders, D.B., Madore, B.F., Neugebauer, G., Danielson, G.E., Elias, J.H., Lonsdale, C.J., & Rice, W.L. 1987, ApJ, 320, 238

Soifer, B.T, Boehmer, L., Neugebauer, G., & Sanders, D.B. 1989, AJ, 98, 766

Stark, A.A., Gammie, C.F., Wilson, R.W., Bally, J., Linke, R.A., Heiles, C., Hurwitz, M. 1992, ApJS, 79, 77

Steidel, C.C. & Hamilton, D. 1992, AJ, 104, 941

Steidel, C.C., Pettini, M., & Hamilton, D. 1995, AJ, 110, 2519

Steidel, C.C., Giavalisco, M., Pettini, M., Dickinson, M., Adelberger, K.L. 1996a, ApJ, 462, L17

Steidel, C.C., Giavalisco, M., Dickinson, M., Adelberger, K.L. 1996b, AJ, 112, 352

Taylor, C.L., Brinks, E., Pogge, R.W., & Skillman, E.D. 1994, AJ, 107, 971

Toomre, A. 1964, ApJ, 139, 1217

van der Hulst, J.M., Skillman, E.D., Bothun, G.D., McGaugh, S.S., & de Blok, W.J.G. 1993, AJ, 106, 548

Veilleux, S., Kim, D.-C., Sanders, D.B., Mazzarella, J.M., & Soifer, B.T. 1995, ApJS, 98, 171

Watson, A.M., Gallagher, J.S., III, Holtzman, J.A., Hester, J.J., Mould, J.R., Ballaster, G.E. 1996, AJ, 112, 534

Whitmore, B.C., Schweizer, F., Leitherer, C., Borne, K., Robert, C. 1993, AJ, 106, 1354

Whitmore, B.C., & Schweizer, F. 1995, AJ, 109, 960

Williams, R.E., Blacker, B., Dickinson, M., Dixon, W.V.D., Ferguson, H.C., Fruchter, A.S., Giavalisco, M., Gilliland, R.L., Heyer, I., Katsanis, R., Levay, Z., Lucas, R.A., McElroy, D.B., Petro, L., Postman, M., Adorf, H.-M., & Hook, R.N. 1996, AJ, 112, 1335

Zhang, X., Wright, M., & Alexander, P. 1993, ApJ, 418, 100

This 2-column preprint was prepared with the AAS LaTeX macros v4.0.

TABLE 1

FOC OBSERVATIONS OF MODERATE REDSHIFT STARBURSTS

Galaxy	z	$m_{\rm F342W}$ (STMAG)	$A_{\rm gal}$[a] (mag)	$A_{\rm int}$[b] (mag)	a_e ($''$)	a/b	D (Mpc)	$\log(L_{\rm bol}/L_\odot)$	R_e (kpc)
QNY1:32	0.4424	19.93	0.16	2.2	0.32	2.03	1338	12.06	1.70
SGP1:10	0.4237	19.87	0.17	0.0	0.20	1.70	1294	11.18	1.14

[a]Galactic extinction evaluated at observed $\lambda = 3403$Å.

[b]Intrinsic extinction evaluated at rest $\lambda_0 = 2320$Å.

TABLE 1

STATISTICS OF SAMPLES AND SUBSAMPLES

(sub)sample	N	$\log(S_{\rm min})$[a]	$\log(S_{e,50})$[a]	$\log(S_{e,90})$[a,b]	$\log(S_{\rm max})$[a]	Description
I.	42	9.31	10.49	11.31	11.94	Total UV sample
I.a	11	9.47	10.53	11.32	11.94	Local UV sample (M95)
I.b	2	9.93	10.10	···	10.26	New moderate z starbursts
I.c	6	9.75	10.23	···	11.39	High-z, Steidel *et al.* (1996a)
I.d	8	10.11	10.70	···	11.46	HDF, Steidel *et al.* (1996b)
I.e	15	9.31	10.12	10.63	10.89	HDF, Lowenthal *et al.* (1997)
I.c-e	29	9.31	10.43	11.21	11.40	All high-z UV subsamples
II.	48	8.23	10.24	10.92	11.50	FIR/Hα sample
II.f	18	9.83	10.52	10.08	11.51	Armus *et al.* (1990)
II.g	30	8.23	9.69	10.57	10.90	Lehnert & Heckman (1995,1996)
III.	38	8.55	10.33	11.71	12.32	21cm obs. Condon *et al.* (1990)
IV.	79	10.27	> 11.92[c]	> 12.73[c]	≥ 13.82[c]	Star clusters in the UV (M95)
V.	34	7.37	7.22	7.69	8.22	Normal disks: Ryder & Dopita (1993)

[a]S_e units are $L_\odot\,{\rm kpc}^{-2}$

[b]Calculated only if (sub)sample size is $N \geq 10$.

[c]lower limits due to large number of R_e upper limits.

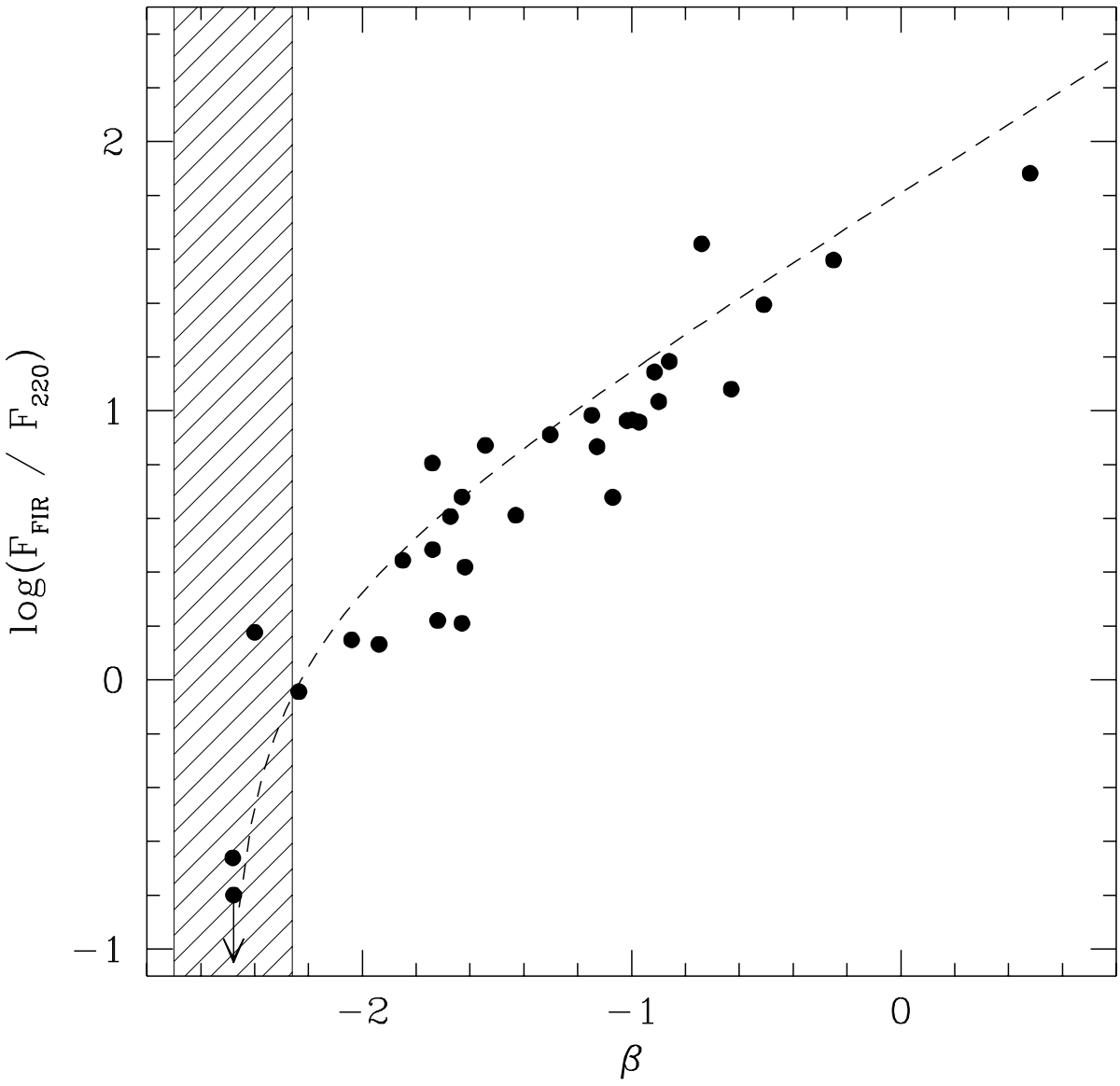

Fig. 1.— The ratio of far-infrared to UV fluxes compared to ultraviolet spectral slope β, adapted from Fig. 6 of M95. The data correspond to UV-selected starbursts observed by IRAS and HST or IUE. Only galaxies with isophotal diameters $D_{25} \leq 5'$ are plotted so as to exclude galaxies with large F_{220} aperture corrections. The hatched region shows the expected β for naked ionizing populations. The dashed line shows the expected relationship for a starburst having an intrinsic $\beta_0 = -2.5$ that is reddened and extincted by a foreground screen of dust with the Calzetti *et al.* (1994) extinction law.

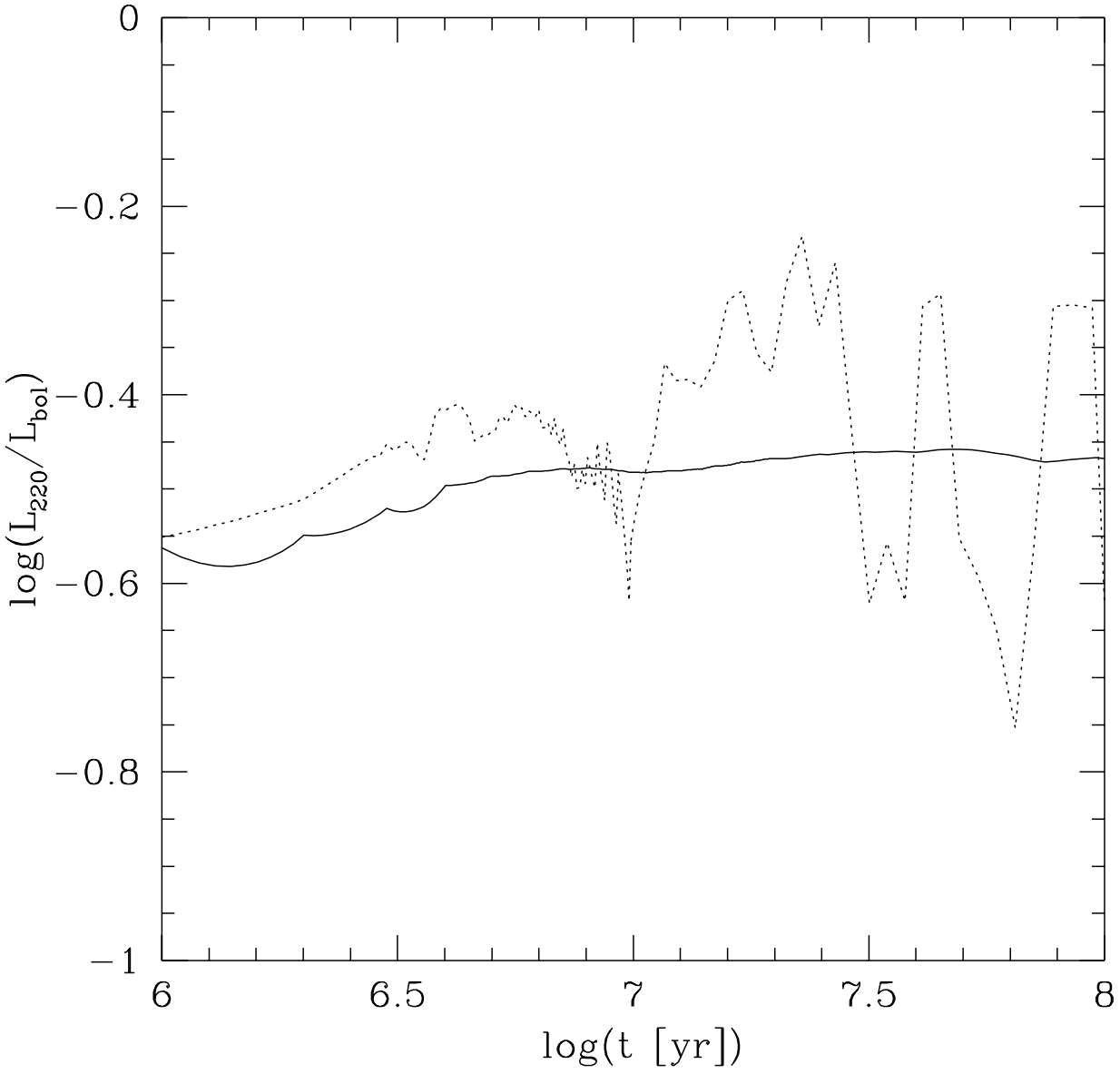

Fig. 2.— The temporal evolution of F220W luminosity as a fraction of the bolometric luminosity for a naked starburst population. The curves were derived from the models of Leitherer and Heckman (1995), assuming a Salpeter (1955) IMF slope, between mass limits of 1 and 100 $\mathcal{M}_\odot$. The effect of extending the mass range down to 0.1 $\mathcal{M}_\odot$ is negligible. The solid line is for a constant star formation rate population, of duration t, and the dotted line is for an instantaneous starburst with age t.

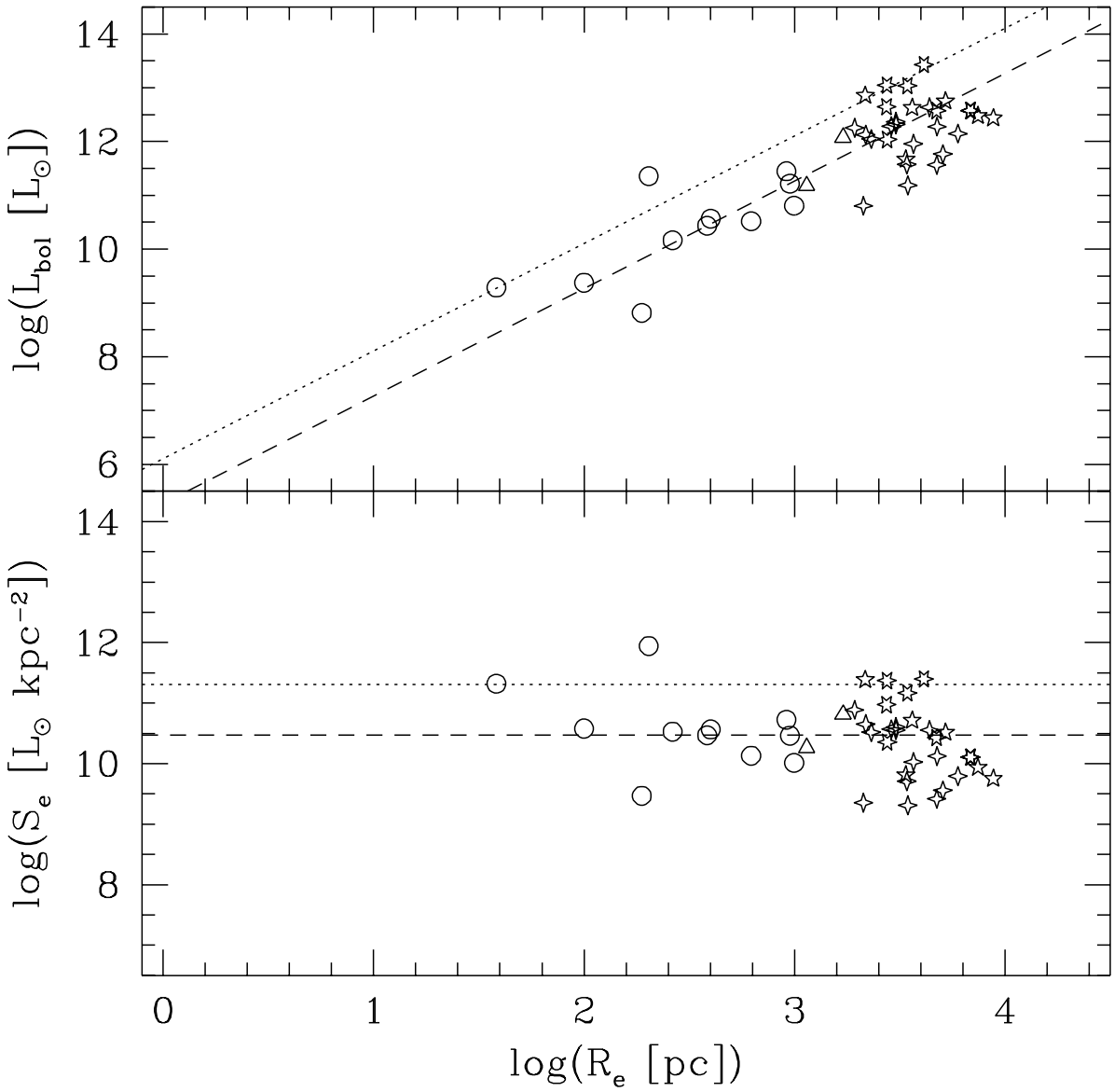

Fig. 3.— Bolometric luminosity $L_{\rm bol}$ and effective surface brightness S_e plotted against effective radius R_e for UV-selected starbursts. The dotted and dashed lines correspond to $S_{e,90}$ and $S_{e,50}$ of the combined sample. The correspondence between symbols and subsamples is as follows: circles - I.a. local starbursts (M95); triangles - I.b. moderate-z starbursts (this work); six pointed stars - I.c. high-z starbursts (Giavalisco *et al.* 1996; Steidel *et al.*, 1996a); five pointed stars - I.d. HDF high-z galaxies Steidel *et al.* (1996b) sample; four pointed stars - I.e. HDF high-z galaxies DEEP sample (Lowenthal *et al.*, 1997).

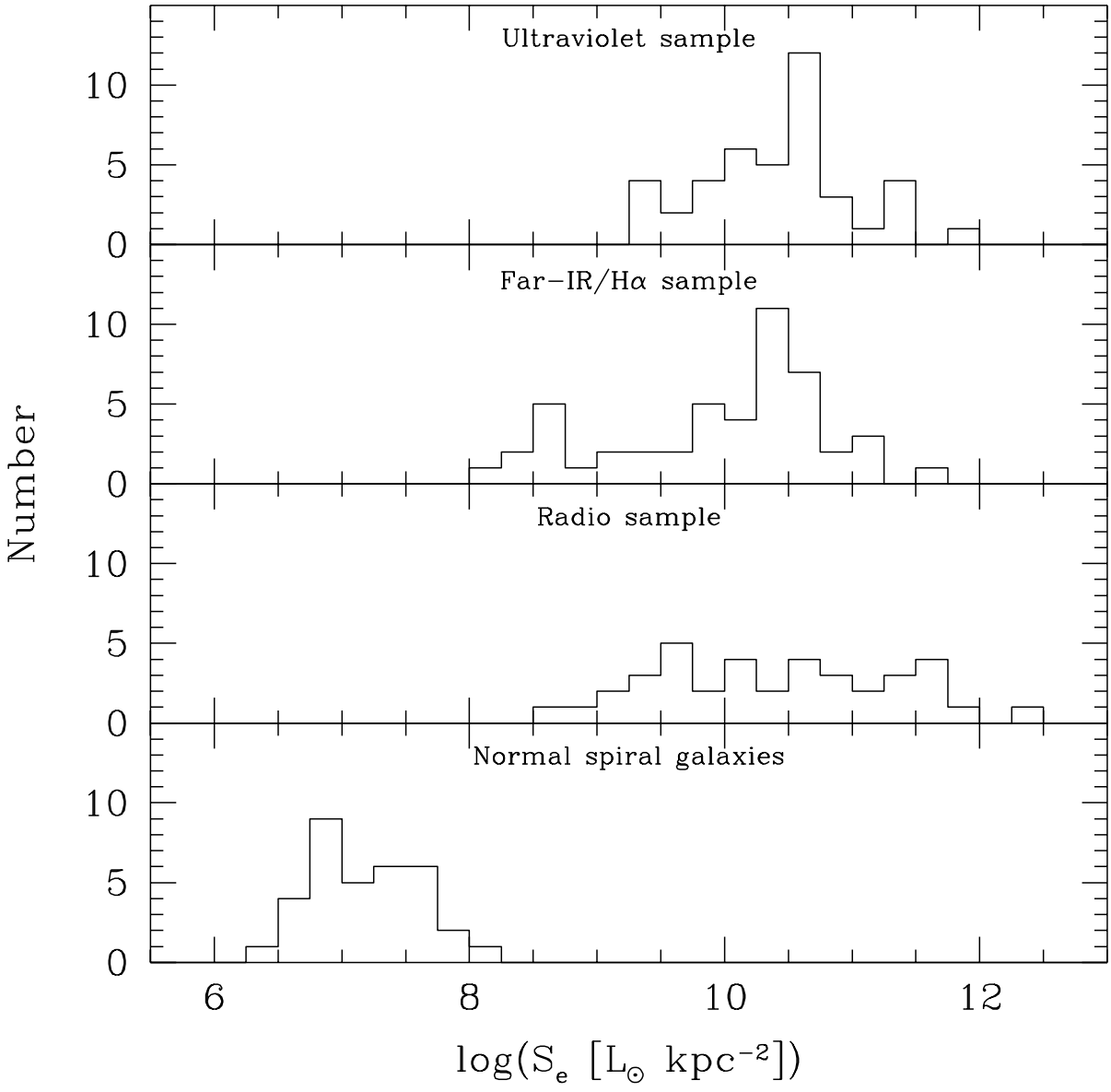

Fig. 4.— Bolometric surface brightness distributions of the UV, FIR/Hα, and radio samples compared to that derived from Hα observations of normal galaxies (Ryder & Dopita, 1993).

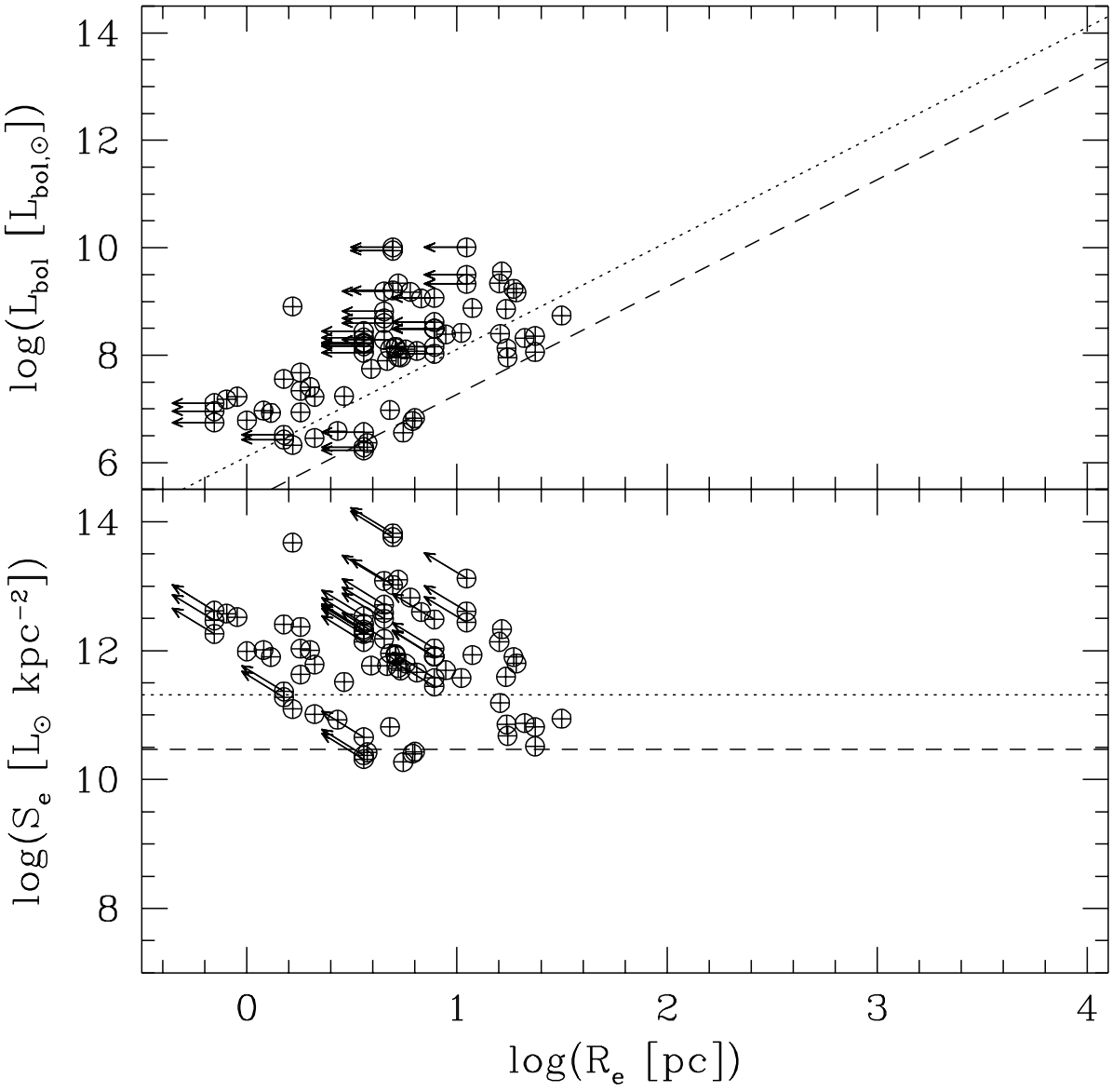

Fig. 5.— Same as Fig. 3 for star clusters within starbursts (from M95). Arrows indicate upper limits to R_e. The dotted and dashed lines have the same position as in Fig. 3.

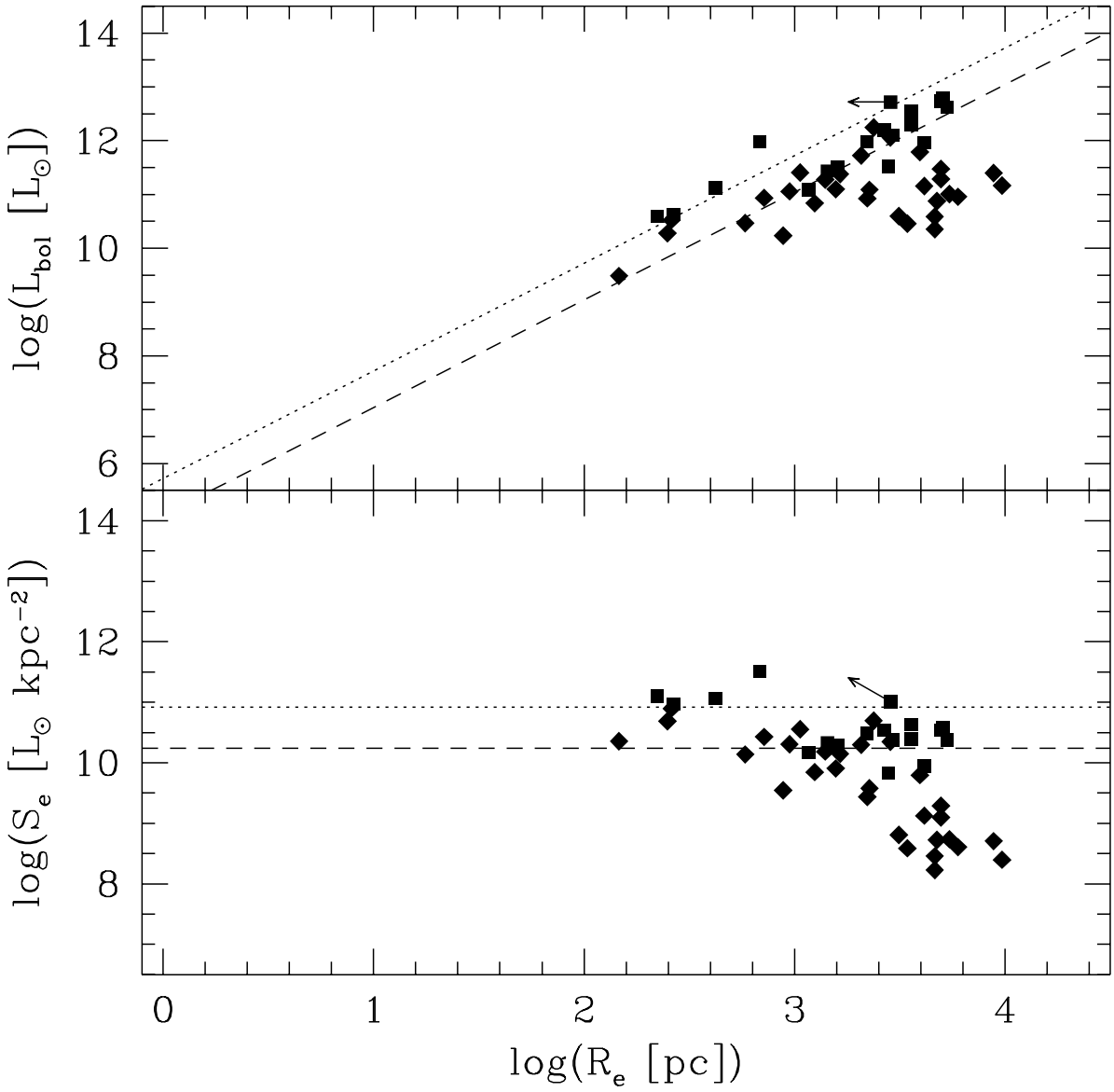

Fig. 6.— Same as as Fig. 3 for the FIR/Hα sample, with the dotted and dashed lines showing $S_{e,90}$ and $S_{e,50}$ limits of this sample. Symbol - subsample correspondence: squares - II.f. (Armus *et al.* 1990); diamonds - II.g. (Lehnert & Heckman, 1995, 1996).

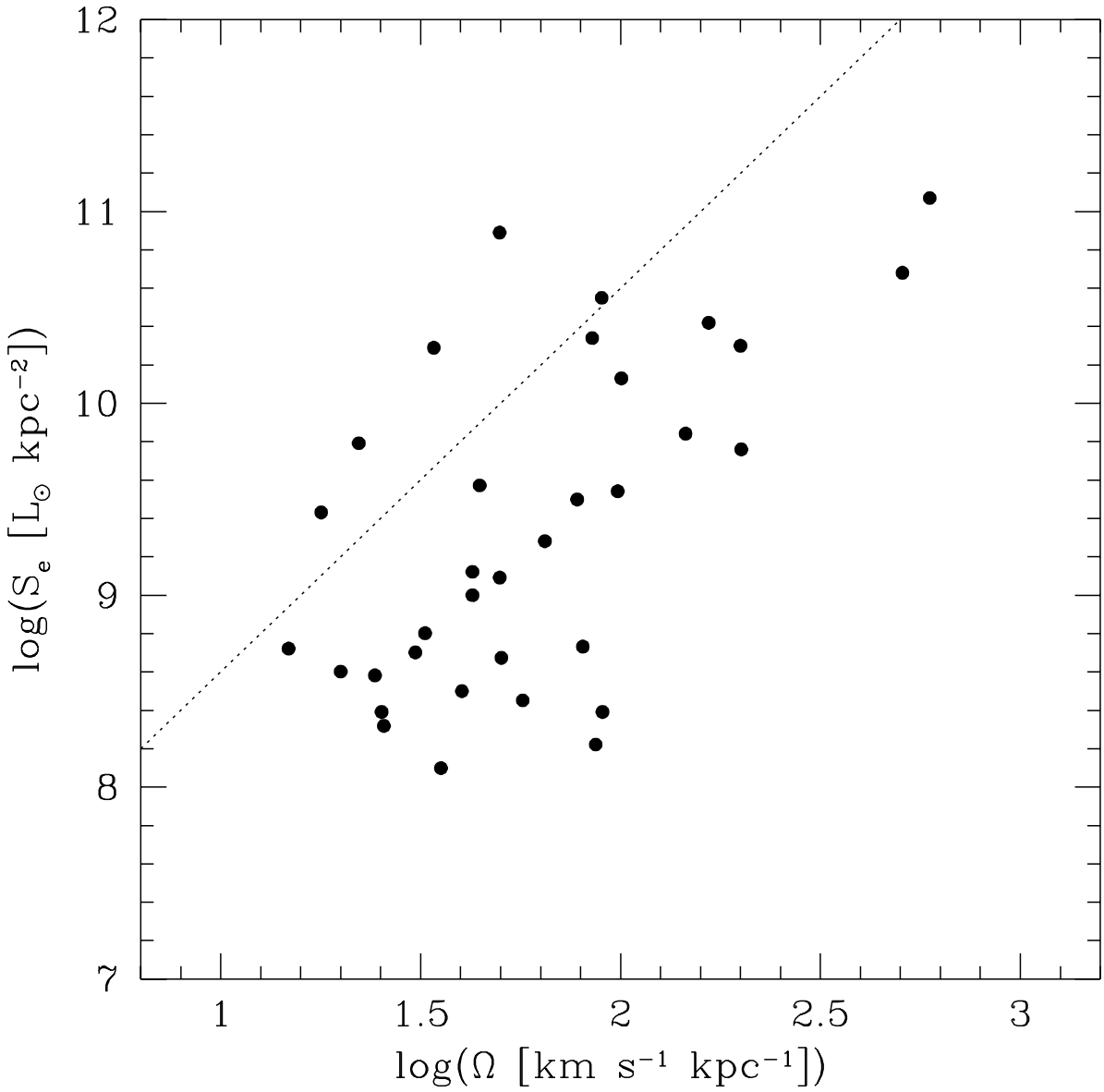

Fig. 7.— Bolometric surface brightness versus angular frequency Ω in the rising portion of the rotation curve for galaxies in subsample II.g (Lehnert & Heckman 1996). Here inclinations were estimated from the axial ratios using $\cos i \approx b/a$. The dotted line shows the expected upper limit expected for gas at Σ_c forming stars over a dynamical time-scale. Since full data are missing for much of subsample II.g we supplemented their kinematics data with published rotation curve data, and have taken $R_e = R_{\rm to}$ (the rotation curve turnover radius) for galaxies with missing R_e (required to estimate S_e). The supplemental data came from the following sources: Armus *et al.* (1990), Carozzi (1977), Carozzi-Meyssonnier (1978), Durret & Bergeron (1988), O'Connell & Mangano (1978), Peterson (1980), Rubin *et al.*(1982), and Zhang *et al.* (1993).

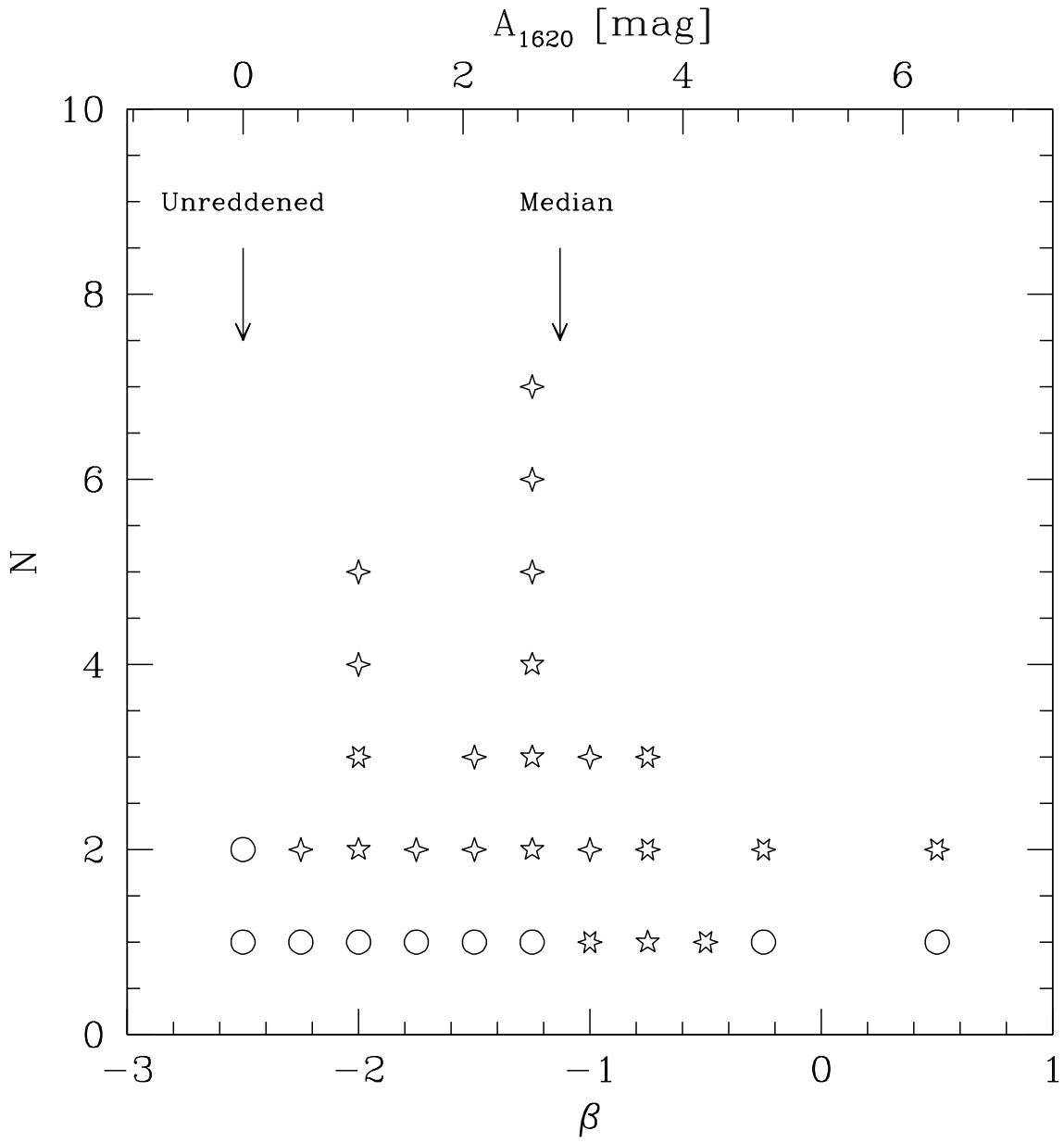

Fig. 8.— Distribution of UV spectral slopes β for the UV sample. The symbols are the same as for Fig. 3. Only one point is plotted where a galaxy resolves into multiple starburst knots.

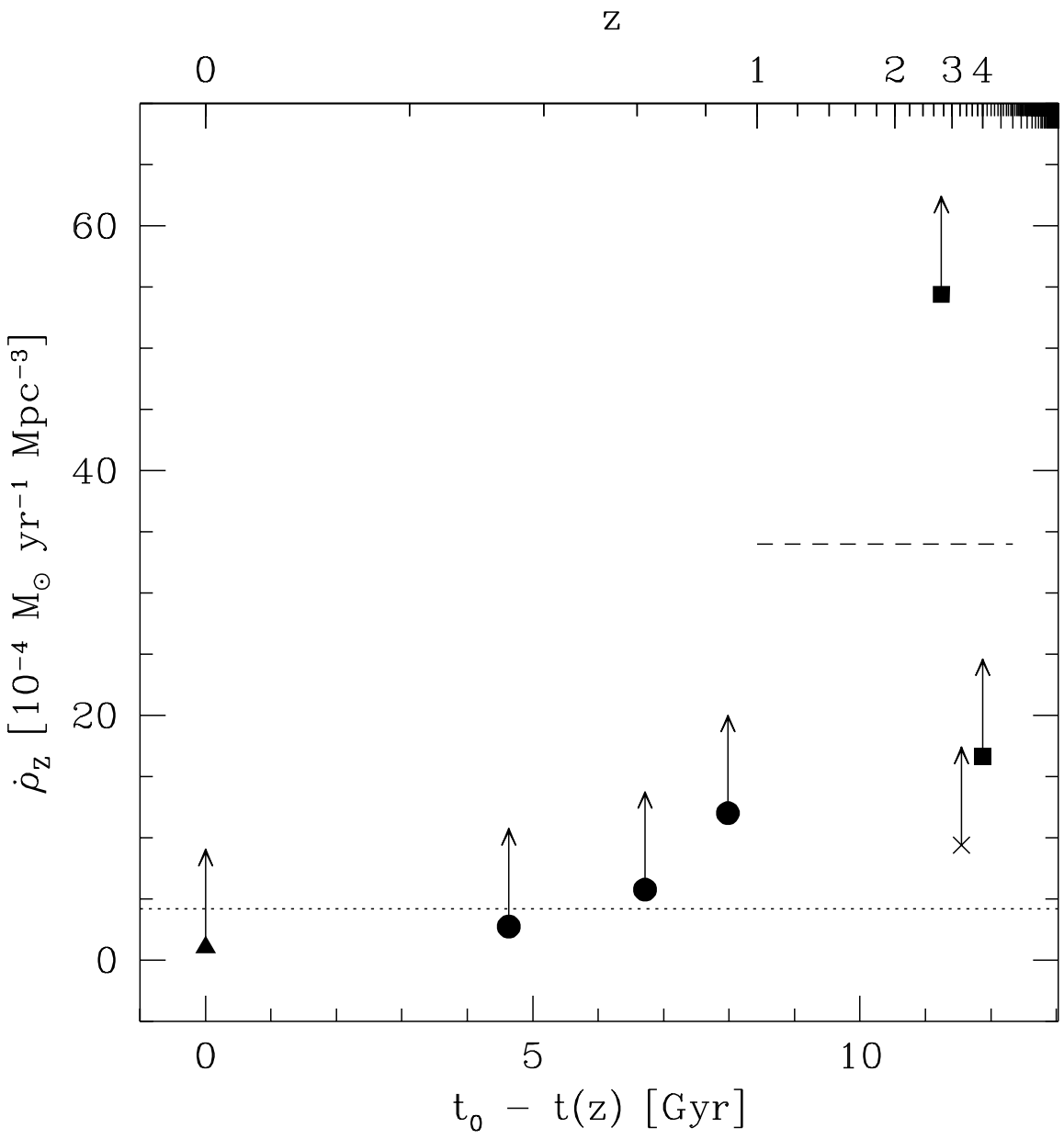

Fig. 9.— Evolution of metal production rate as a function of look-back time (bottom axis), and redshift (top axis). The symbol correspondence is as follows: squares - Madau *et al.* (1996); x - Steidel *et al.* (1996a); circles - Lilly *et al.* (1996); triangle - Gallego *et al.* (1995). The data points are all lower limits. For $z > 2$ this is because completeness corrections have not been made. For $z < 1$ this is because no dust extinction corrections have been made. The dotted line shows the Hubble time averaged metal production rate estimated by Madau *et al.* (1996). The dashed line segment shows the mean metal production rate during the epoch of elliptical galaxy formation as estimated by Mushotzky & Loewenstein (1997).